# Nature of the Mantle Plume Under the Emeishan Large Igneous Province: Constraints From Olivine-Hosted Melt Inclusions of the Lijiang Picrites

**7 authors**, including:

Lei Zhang
Chinese Academy of Sciences
**3** PUBLICATIONS **22** CITATIONS

SEE PROFILE

Zhong-Yuan Ren
Chinese Academy of Sciences
**80** PUBLICATIONS **1,715** CITATIONS

SEE PROFILE

Le Zhang
Chinese Academy of Sciences
**112** PUBLICATIONS **1,059** CITATIONS

SEE PROFILE

Sheng-Ping Qian
Tongji University
**23** PUBLICATIONS **315** CITATIONS

SEE PROFILE

**Some of the authors of this publication are also working on these related projects:**

Project — LA-MC-ICPMS View project

Project — Crustal growth and evolution View project

**Key Points:**
- Highly heterogeneous Pb isotope compositions of olivine-hosted melt inclusions are found in the Lijiang picrites
- GLOSS II-like subduction sediments are responsible for the enriched mantle 1-like component in the source of the Emeishan large igneous province (LIP)
- Thermal variation of the mantle plume controlled the types and distribution of basaltic magmas in the Emeishan LIP

# Nature of the Mantle Plume Under the Emeishan Large Igneous Province: Constraints From Olivine-Hosted Melt Inclusions of the Lijiang Picrites

Lei Zhang[1,2,3], Zhong-Yuan Ren[1,2,4] , Le Zhang[1,2] , Ya-Dong Wu[1,4,5], Sheng-Ping Qian[1,6] , Xiao-Ping Xia[1,2,4] , and Yi-Gang Xu[1,2,4]

[1]State Key Laboratory of Isotope Geochemistry, Guangzhou Institute of Geochemistry, Chinese Academy of Sciences, Guangzhou, China, [2]CAS Center for Excellence in Deep Earth Science, Guangzhou, China, [3]College of Earth and Planetary Sciences, University of Chinese Academy of Sciences, Beijing, China, [4]Institutions of Earth Science, Chinese Academy of Sciences, Beijing, China, [5]State Key Laboratory of Lithospheric Evolution, Institute of Geology and Geophysics, Chinese Academy of Sciences, Beijing, China, [6]State Key Laboratory of Marine Geology, Tongji University, Shanghai, China

**Abstract** Olivine-hosted melt inclusions have the potential to provide direct evidence about the nature of the mantle sources of magmas. In this study, we report the major and trace element and Sr–Nd–Pb–Hf isotope compositions of the Lijiang picrites from the Emeishan large igneous province, as well as major and trace element and Pb isotopic compositions of olivine-hosted melt inclusions in the picrites. Using these data, we infer the nature of the mantle sources for the Lijiang high-Ti picrites (Ti/Y = 645–654), and compare them with the Dali low-Ti picrites (Ti/Y = 351–408). Lijiang melt inclusions have highly heterogeneous Pb isotope compositions ($^{208}Pb/^{206}Pb$ = 2.015–2.201, $^{207}Pb/^{206}Pb$ = 0.812–0.882, 260 Ma age-corrected) that overlap the majority of the fields from FOZO to enriched mantle 1 (EM1). The primitive mantle-normalized trace element patterns of these melt inclusions reveal an enriched composition with depletions in Ba, Nb, Ta, Zr, and Hf. We suggest that an old recycled GLOSS II-like sediment was probably the main component that imparted the EM1 signature into the sources of the Lijiang picrites. Furthermore, we reverse calculated the mantle potential temperature ($T_p$) beneath Lijiang and Dali using the Al-in-ol temperature. The estimated mantle $T_p$ beneath Lijiang is lower than Dali. We infer that the Lijiang picrites might have originated from the mantle plume with lower thermal energy, corresponding to the waning stage of the axis of the Emeishan mantle plume. Our study suggest that high-Ti magmas of the Emeishan large igneous province were derived from those parts or stages of the mantle plume with lower thermal energy.

## 1. Introduction

Large igneous provinces (LIPs) result from intensive large-scale magmatism in which vast volumes ($>0.1 \times 10^6$ km$^3$) of magma were erupted over a short duration (<5 Myr; Bryan & Ernst, 2008). Some LIPs are thought to have been associated with mantle plumes and are therefore of high importance to the study of the Earth's mantle. The Emeishan LIP has received much research attention because it hosts world-class Fe–Ti–V oxide deposits and is considered to have contributed to the end-Guadeloupian mass extinction (Shellnutt et al., 2009; Shellnutt & Jahn, 2010; Song et al., 2013; J. Yang et al., 2015; Y. Zhang et al., 2013; H. Zhong et al., 2011). The Emeishan LIP is generally accepted to have been related to the activity of a mantle plume (Ali et al., 2010; Chen et al., 2015; Hanski et al., 2010; He et al., 2003; J. Liu et al., 2017; K. Putirka et al., 2018; Ren et al., 2017; Song et al., 2008; Tao et al., 2015; R. Xu et al., 2020).

With respect to LIPs, the petrogenesis of high- and low-Ti magmas is a topic of continuing research interest (e.g., Hergt et al., 1991; Jourdan et al., 2007; Kamenetsky et al., 2017). The Ti/Y ratios of picrites and basalts in the Emeishan LIP lie mostly within the ranges of 200–800. Y. G. Xu et al. (2001) found systematic differences in magmatic compositions between different Ti/Y, and classified the picrites and basalts in the Emeishan LIP into low-Ti (Ti/Y < 500) and high-Ti (Ti/Y > 500) series. This classification method has been widely used to define high-Ti and low-Ti magmas in subsequent studies of the Emeishan LIP. However, an increasing number of data have shown that the Ti/Y ratios of basaltic magmas in the Emeishan LIP are transitional and vary between low-Ti and high-Ti groups (Kamenetsky et al., 2012; Ren et al., 2017; Shellnutt

& Jahn, 2011). Thus, it should be aware that high-Ti and low-Ti series are not two distinct groups but a continuous spectrum of compositions.

Many researchers have suggested that high-Ti magmas were derived directly from low-degree melting of a mantle plume, whereas low-Ti magmas were derived from high-degree melting of sub-continental lithospheric mantle (SCLM) or by contamination by crustal material (Fan et al., 2008; C. Y. Wang et al., 2007; Xiao et al., 2004; Y. G. Xu et al., 2001; Zhou et al., 2008). Opposing opinions maintain that high-Ti magmas were derived from SCLM, whereas low-Ti basalts were derived from the mantle plume (J. F. Xu et al., 2007). Kamenetsky et al. (2012) considered that both low-Ti and high-Ti basalts were derived from SCLM and that high-Ti magmas were derived from a garnet pyroxenite source, and low-Ti magmas from a peridotite source. Conversely, Shellnutt and Jahn (2011) proposed that high-Ti and low-Ti basaltic magmas are likely derived from the same source and that the geochemical differences between these two types can be caused by different degrees of partial melting and assimilation of crustal material. Hou et al. (2011) argued that the different Ti/Y ratios of magmatic rocks are not a reflection of different sources but rather of differential fractional crystallization of Fe–Ti oxides magmas of the Emeishan LIP. Ren et al. (2017) and L. Zhang et al. (2019) proposed that the Emeishan LIP was derived from a relatively homogeneous pyroxenite source and that the mixing of melts from different depths and melting degrees of the mantle plume may explain the compositional variability of magmas. R. Xu et al. (2020) argued that a relatively homogeneous peridotitic mantle plume source can explain the compositional ranges of olivines and picrites in the Emeishan LIP.

Recently, some studies have proposed that recycled materials in the Emeishan mantle plume played a key role in producing the observed compositional diversity of the Emeishan LIP (Bai et al., 2014; Hou et al., 2013; C. Yang & Liu, 2019; Yu et al., 2014; L. Zhang et al., 2019). C. Yang and Liu (2019) and L. Zhang et al. (2019) estimated an oceanic crust component of ~15% in the source of the Emeishan LIP. Using the Zn isotopes of basalts, C. Yang and Liu (2019) inferred that marine carbonate components were not present in the source of the Emeishan basalts. There is a general consensus that the recycling of oceanic and continental crust into the mantle, which may involve different sedimentary components, results in the enrichment of the mantle and the formation of different enriched mantle end-members (Hofmann, 2003; Stracke, 2012; White & Hofmann, 1982). Although the proportion of the recycled component is relatively low, these crust-like and sedimentary components exert a dominant control on the geochemical heterogeneity of the mantle (e.g., Willbold & Stracke, 2006). Thus, determining the specific components that accompanied oceanic crust recycled into the mantle of the Emeishan LIP, the recycling time, and their contributions to the compositional characteristics of magmas should provide insights into the origins of the enriched mantle end-member.

Picrites in the Emeishan LIP contain olivines with high Fo values (e.g., Fo contents of olivnes in Lijiang picrites up to 91.6 mol%) and should provide key information on the origin of Emeishan LIP lavas. Melt inclusions enclosed in early formed olivine crystals are generally regarded as representing nearly unevolved, primary melt compositions and can preserve more information about mantle sources compared with the whole-rock compositions (Kent, 2008; Norman et al., 2002; Sobolev, 1996). Therefore, investigation of melt inclusions should provide close constraints on the sources and petrogenesis of magmas of the Emeishan LIP. Typically, trace element compositions are the collective consequence of influences of the source component, melting processes, and minerals crystallization. Isotopic compositions also have multiple petrogenesis (Stracke, 2012). Therefore, combining trace element contents with isotopic compositions is an effective approach for constraining the nature of the source component. For the Emeishan LIP, only data from the Dali picrites (Ti/Y = 358–409, which belongs to low-Ti series according to the classification method of Ti/Y = 500) have been reported with regard to major and trace elements and Pb isotopic compositions of melt inclusions (L. Zhang et al., 2019).

The Lijiang picrites have Ti/Y = 609–807 (Hanski et al., 2010; Song et al., 2001; Z. C. Zhang et al., 2006) and thus belong to the high-Ti series in the Emeishan LIP. The Lijiang picrites have high MgO contents (up to 27.8 wt.%), and previous studies have considered that the picrites are originated from melting of the hot mantle plume head of the Emeishan LIP (He et al., 2010; Z. C. Zhang et al., 2006). In this study, we present details of a study of the major and trace element and Pb isotopic research on the Lijiang olivine-hosted melt inclusions, and the major and trace element as well as the Sr, Nd, Pb, Hf isotopic compositions of the host picrites. We report highly heterogeneous Pb isotopic compositions of melt inclusions in the Lijiang picrites,
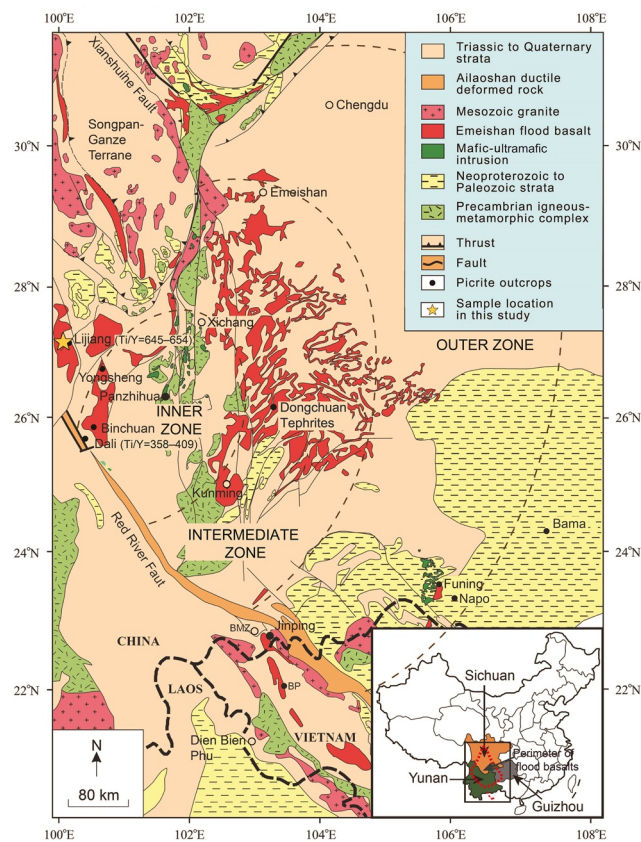
**Figure 1.** Geological map showing the distributions of basalts and picrites in the Emeishan large igneous province (Emeishan LIP) (modified after Kamenetsky et al., 2012). The locations of the picrites found in the Emeishan LIP are shown by black circles. Brown dashed curves are the estimated boundaries of the inner, intermediate, and outer zones (He et al., 2003). The Ti/Y ratios of the Lijiang and Dali picrites in this study are also shown. LIP, large igneous province.

which provide direct evidence of an enriched mantle 1 (EM1) end-member component in the source of the Emeishan LIP. We discuss the origin of the EM1 signature and identify the source of the Lijiang picrites, and compare the compositional characteristics of the Lijiang olivine-hosted melt inclusions with those of Dali. We also analyze the spinel inclusions and host olivines in the Lijiang and Dali picrites, and present the results of Al-in-ol thermometer of olivines from Lijiang and Dali, and estimate the mantle potential temperature ($T_p$) differences beneath Lijiang and Dali. Finally, we combined with the geochemical data, thermodynamic variation in the mantle plume, and the spatial distributions of different types of magmas to construct an integrated model of the genesis of high-Ti and low-Ti magmas in the Emeishan LIP.

## 2. Geological Background and Sampling

The Emeishan LIP is in the western margin of the Yangtze plate and adjacent to the eastern margin of the Tibetan plate, SW China (Chung & Jahn, 1995; Figure 1). Lavas of the Emeishan LIP are also found in Vietnam, the Qiangtang area of Tibet, and west of Guangxi (Anh et al., 2011; Chung et al., 1998; Fan et al., 2008; Hanski et al., 2004; X. J. Liu et al., 2016; C. Y. Wang et al., 2007). The southwestern part of the Emeishan LIP has been eroded as a result of the collision of the Indian and Eurasian continents during the Cenozoic (Ali et al., 2004; Zhou et al., 2006). Flood basalts of the LIP cover an area of more than $2.5 \times 10^5$ km$^2$ and have an estimated volume of $>3 \times 10^5$ km$^3$ (Y. G. Xu et al., 2001). Eroded limestone of the early Permian Maokou Formation, which is unconformably overlain by Emeishan LIP lavas, is considered to record the effect of the rising mantle plume head (He et al., 2003). According to the amount of crustal uplift inferred from the differential extent of erosion, the Emeishan LIP is divided into inner, intermediate, and outer zones (He et al., 2003; Figure 1). The thickness of the Emeishan volcanic sequences varies systematically from more than 5,000 m in the inner zone to several hundred meters in the outer zone (Y. G. Xu et al., 2004; Zhu et al., 2018). Acid rocks comprising mainly rhyolites and granites coexisting with basalts represent the late stage of magmatic activity (Y. G. Xu et al., 2010). Picrites are rare, with outcrops of these rocks being found predominantly in Lijiang, Dali, Pingchuan, Yongsheng, Song Da, and Yumen (Hanski et al., 2010; Kamenetsky et al., 2012; Ren et al., 2017; Tao et al., 2015; Y. D. Wu et al., 2018; Yu et al., 2017, 2020; Yao et al., 2019; Z. C. Zhang et al., 2006, 2008). The main phase of magmatism of the Emeishan LIP occurred at ca. 260 Ma (Li et al., 2017; Y. T. Zhong et al., 2014, 2020), and lasted at least 6 Myr (Shellnutt et al., 2020). These eruptions might have led to the extinction event at the end-Guadalupian (Wignall et al., 2009; Y. C. Xu et al., 2018; J. Yang et al., 2015; Y. Zhang et al., 2013).

Picrites in this study were sampled near Lijiang city (26°53′03.075″N, 100°10′55.643″E). They occur as several weathered outcrops interspersed with aphyric basalt/basaltic lavas and overlain by Triassic sandstones. The picrites are located in the lower portion of the volcanic section. They are porphyritic, and the phenocrysts are olivine (40 vol.%). Most of these olivine phenocrysts are euhedral with diameters of 0.5–2 mm, and a few grains can reach 4–5 mm. Intense serpentinization and chloritization occur along rims and fractures, but the cores of many olivines remain fresh, and the euhedral outlines are well preserved (Figure S1). Melt inclusions and Cr-spinel inclusions can be found enclosed in these fresh olivine cores. Most of the melt inclusions are oval, with sizes ranging from 10 to 50 μm in diameter (Figure S1f). Filamentous or acicular daughter minerals can be found in melt inclusions and early crystallized Cr-spinel coexists in some melt inclusions. Cr-spinel inclusions are euhedral, semi-opaque to opaque, and randomly distributed in olivine crystals. Their size is commonly less than 30 μm in diameter. The groundmass of picrites is composed mainly of glass and fine-grained olivine, diopside and plagioclase.

## 3. Analytical Methods

In this study, we analyzed major and trace elements contents and Sr–Nd–Pb–Hf isotopic compositions of samples of the Lijiang picrites, as well as major and trace element and Pb isotopic compositions of olivine-hosted melt inclusions in the picrites. A total of 165 pairs of melt inclusions (>25 μm) and host olivines were analyzed with EMPA. The trace elements compositions of melt inclusions (>35 μm) were analyzed with a Cameca IMS 1280HR secondary ion mass spectrometry instrument, and Pb isotopes were analyzed with a Neptune Plus multi-collector inductively coupled plasma–mass spectrometry (MC–ICP-MS) instrument coupled with a RESOlution M-50 193 nm laser ablation system (L. Zhang et al., 2014). We also analyzed the major element compositions of spinel inclusions in olivines and the major, minor and trace element compositions of host olivines for both spinels and melt inclusions with EMPA. The olivines were analyzed following the method of Sobolev et al. (2007). The MongOL (Batanova et al., 2019) was analyzed to estimate accuracy and precision. Details of the analytical methods used, and data generated, are summarized in the supporting information. The analytical results of standards are consistent with recommended values or previous studies within analytical error (Cao et al., 2019; Elburg et al., 2005; Jochum et al., 2011; Tanaka et al., 2000; Todt et al., 1996; Vance & Thirlwall, 2002; Weis et al., 2005; F. Y. Wu et al., 2006; Xie et al., 1989).

## 4. Results

### 4.1. Major and Trace Elements and Isotopic Compositions of the Lijiang Picrites

The major element compositions of the Lijiang picrites (in Table S1) are homogeneous, with high MgO (25.7–27.7 wt.%) and $TiO_2$ (1.19–1.32 wt.%) contents and low $Al_2O_3$ (6.20–7.10 wt.%) contents (Figure 2a). These picrites have total alkalis ($Na_2O+K_2O$) of 0.93–1.11 wt.% and $SiO_2$ of 44.3–45.8 wt.% (Figure S2; Le Bas et al., 1986). The Lijiang picrites exhibit high Ti/Y ratios (Ti/Y = 645–654), which group them with the high-Ti series in the Emeishan LIP. The Lijiang picrites are strongly enriched in light rare earth elements (REEs) relative to heavy REE ($(La/Yb)_N$ = (6.60–6.71), where subscript N denotes chondrite normalization) in chondrite-normalized REE diagrams (Figure S3). Mobile elements (such as Rb, Ba, Sr and Pb) exhibit greater variability in composition relative to neighboring elements, which reflects the influence of later alteration. The Lijiang picrites are characterized by uniform and depleted Sr ($^{87}Sr/^{86}Sr_i$ = 0.70420–0.70429), Nd ($\varepsilon_{Nd(t)}$ = +3.27–+3.48) and Hf ($\varepsilon_{Hf(t)}$ = +7.7–+8.0) isotopic compositions (Table S2), which are intermediate in comparison with those of typical oceanic island basalts (OIBs) (Figure S4). In the $\varepsilon_{Nd(t)}$ versus $\varepsilon_{Hf(t)}$ diagram, the Lijiang picrites plot within the mantle array (Figure S4). These samples also have homogeneous and intermediate Pb isotopic compositions ($^{206}Pb/^{204}Pb_i$ = 18.63 ± 0.17; $^{207}Pb/^{204}Pb_i$ = 15.63 ± 0.08; $^{208}Pb/^{204}Pb_i$ = 38.83 ± 0.20; mean values ± 2SD). In general, no pronounced variations are found in the major and trace element or isotopic compositions of these picrites.

### 4.2. Major and Trace Elements of Olivines and Melt Inclusions

The olivines in the Lijiang picrites have a wide range of compositions, with Fo values ranging from 84.4 to 91.6 mol%. The olivines have high CaO (>0.3 wt.%) and $Al_2O_3$ (>0.03 wt.%) contents that differ from those of mantle-derived olivine xenocrysts (CaO<0.1 wt.%, $Al_2O_3$ < 0.01 wt.%; Foley et al., 2013). In addition, numerous Cr-spinels and melt inclusions are enclosed in olivines (Figure S1d), which also indicates that these olivines are of magmatic origin (Kamenetsky et al., 2017). After melt inclusions are entrapped in olivine, olivine and other daughter minerals crystallize in the melt inclusions and/or along the inner wall of the olivine as temperature decreases, and this process can significantly modify the compositions of inclusions (Kent, 2008; Nielsen et al., 1998; Sobolev, 1996). In addition, "Fe-loss" occurs in the melt inclusions because of Mg–Fe exchange and re-equilibration between olivine and melt inclusions (Danyushevsky et al., 2000, 2002; Sobolev et al., 2000). Melt inclusions would still inherit low $FeO_T$ and high MgO contents even after the homogenization process. This phenomenon is more obvious in the melt inclusions of high-Fo olivine (with FeO as low as 4.5 wt.%; Figure S5). To correct for this influence, we applied the method of Danyushevsky et al. (2000), and used the model of Ford et al. (1983) and PETROLOG 3 software (Danyushevsky & Plechov, 2011) to reconstruct the compositions of the studied melt inclusions to be in equilibrium with the host olivines (data and parameters are supplied in Table S4 and S7).
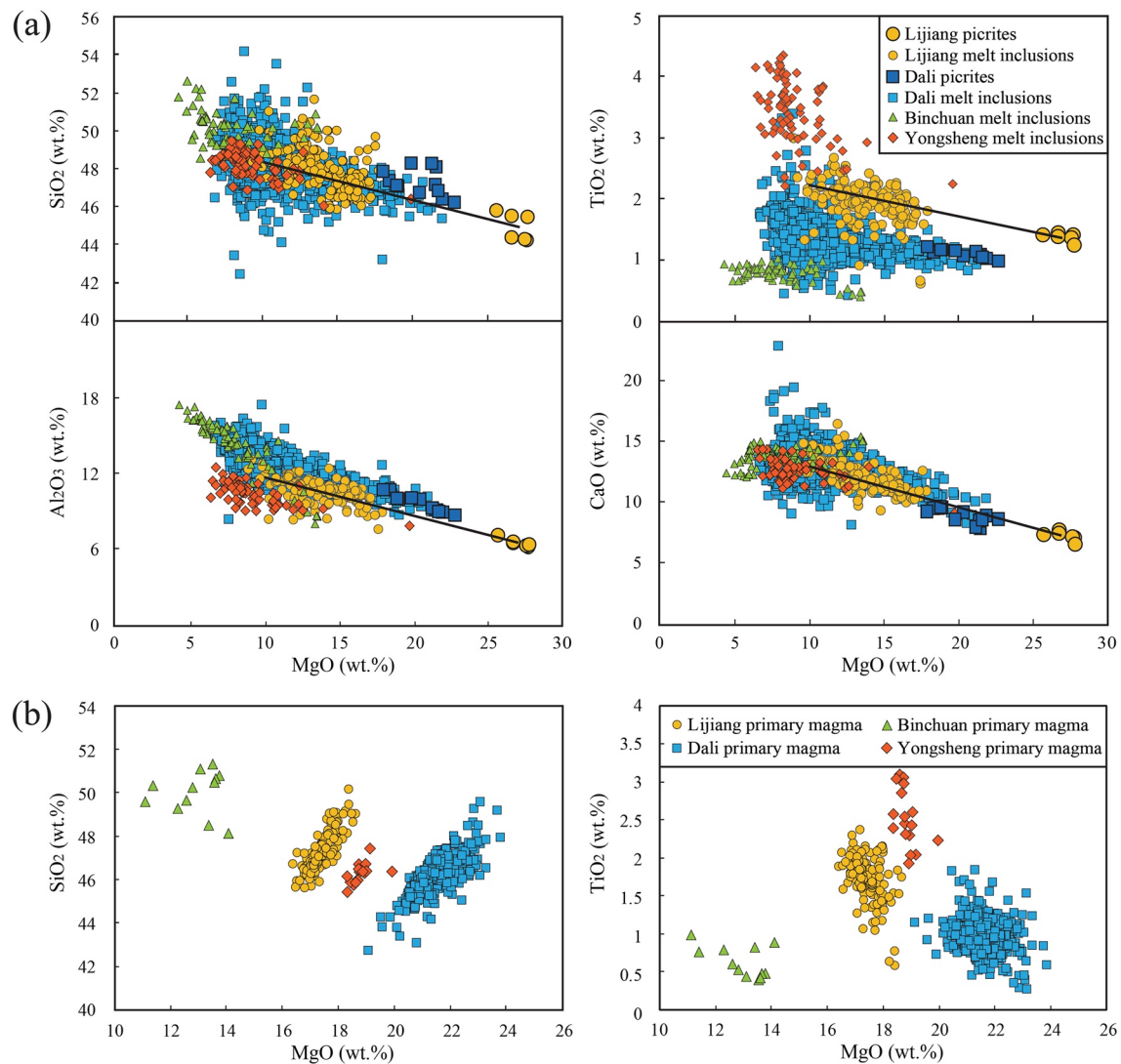
**Figure 2.** Major oxides versus SiO₂ for (a) Emeishan melt inclusions and host picrites and (b) Emeishan primary magmas. (a) The large yellow circles represent host picrites, and the small yellow symbolize the compositions of Lijiang melt inclusions. The melt inclusion compositions were corrected for post-entrapment with the PETROLOG 3 software (Danyushevsky & Plechov, 2011) and the olivine–melt model of Ford et al. (1983). The blue squares are the compositions of Dali picrites and melt inclusions (data from Ren et al., 2017 and L. Zhang et al., 2019); average Ti/Y of melt inclusions is 396). The data for the Binchuan picrites (average Ti/Y = 297, low-Ti end-member) and Yongsheng picrites (average Ti/Y = 790, high-Ti end-member) are shown for comparison (data from Kamenetsky et al., 2012). The black line traces the olivine fractionation trends calculated by gradually removing olivine compositions from the average composition of host picrites. (b) Primary magmas of picrites in Lijiang, Dali, Binchuan, and Yongsheng estimated with respective melt inclusion compositions. The primary magma composition was estimated using the "reverse crystallisation" of the PETROLOG 3 software (Danyushevsky & Plechov, 2011) by incrementally adding 0.1% olivine in Fe–Mg equilibrium at each calculation until the composition of melts equilibrated with the most forsteritic olivine found in each area [Lijiang: Fo₉₁.₆ (this study), Dali: Fo₉₃.₅ (Hanski et al., 2010), Binchuan: Fo₉₁.₂ (Kamenetsky et al., 2012), Yongsheng: Fo₉₁.₇ (Kamenetsky et al., 2012)].

The MgO contents of the corrected melt inclusion compositions range from 8.94 to 17.93 wt.% and are substantially lower than the contents of the host whole rocks (Figure 2a). Melt inclusions in the Lijiang picrites have high $TiO_2$ and low $Al_2O_3$ contents, showing affinity to the melt inclusion compositions of the Yongsheng picrites (Ti/Y = 787–794, from Kamenetsky et al., 2012). Trace element patterns of the averaged melt inclusions are generally subparallel to those of their host whole rocks (Figure 3a). Compared with the compositions of Dali melt inclusions, the Lijiang melt inclusions exhibit lower Ba and Th contents and do not show Nb–Ta depletion and Pb enrichment (Figure 3a). The Lijiang melt inclusions have mantle-like to lower Nb/U (16.0–55.5, average = 32.7) and Ce/Pb (7.0–24.3, average = 14.8 ratios compared with typical OIBs (Nb/U = 47 ± 10, Ce/Pb = 25 ± 10; Hofmann et al., 1986), and have higher Th/U ratios (3.2–6.0,
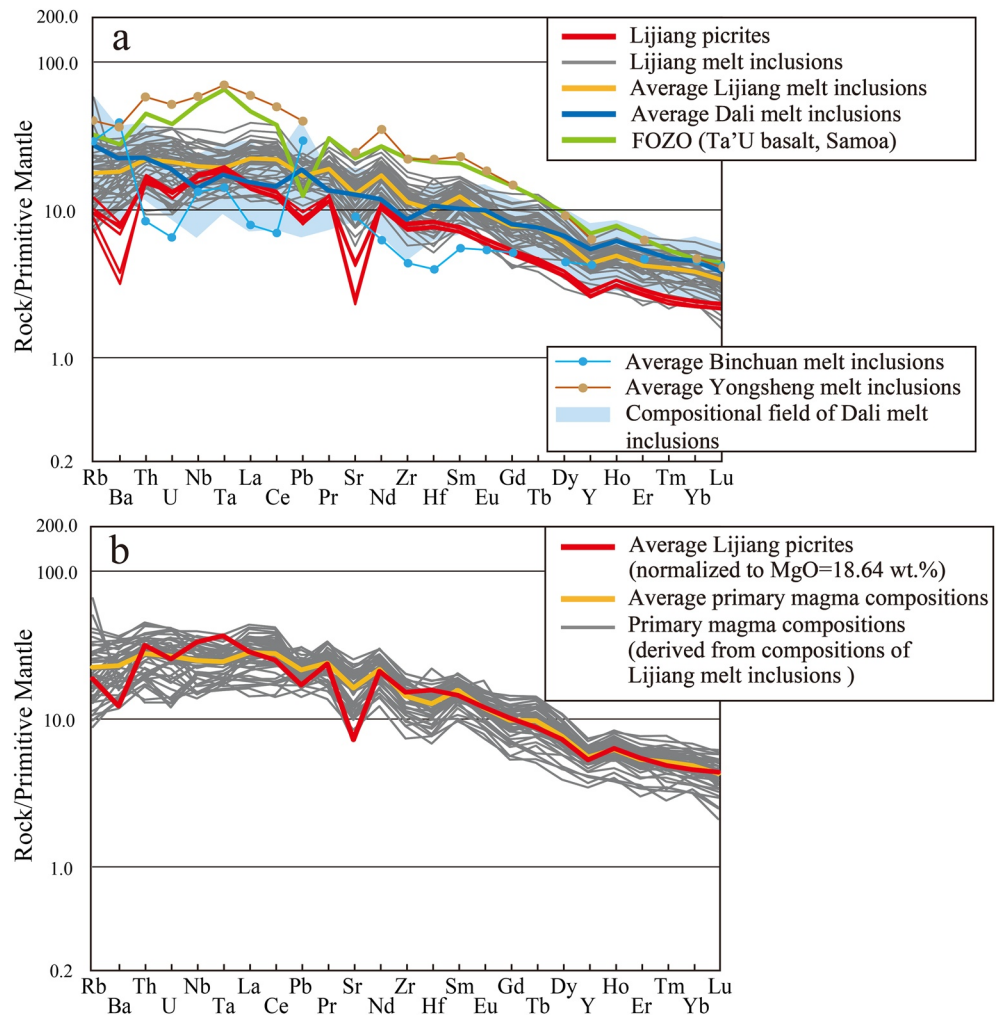
**Figure 3.** Primitive mantle-normalized (McDonough & Sun, 1995) trace element patterns for Lijiang melt inclusions and picrites. (a) The patterns of the picrites (red lines) and the average melt inclusion compositions (yellow line). The light-blue field is the compositional field of melt inclusions in Dali picrites (L. Zhang et al., 2019). The green line is the average composition of Ta'U basalts (Samoa Islands) reported by Hart and Jackson (2014), whose source is considered to be the FOZO mantle end-member. The data for the Binchuan picrites and Yongsheng picrites are from Kamenetsky et al. (2012). (b) Trace element patterns of the primary magma compositions. The trace element compositions of primary magma are also derived from compositions of the Lijiang melt inclusions. The calculation method is identical to that for major elements and is explained in Table S9. The red line is the pattern of average Lijiang picrites normalized to MgO = 18.64 wt.% (the highest MgO of the primary magma).

average = 4.2) relative to the bulk Earth (Th/U = 3.9; Galer & O'Nions, 1985) but evidently lower Th/U than the lavas from Pitcairn Island (Th/U = 4.4–14.4; Eisele et al., 2002). The trace element ratios of the studied melt inclusions also present wide compositional variability. For example, the Ti/Y and $(La/Yb)_N$ ratios of the melt inclusions range from 318 to 998 and from 3.87 to 9.02, respectively. Nevertheless, the mean values (Ti/Y = 669; $(La/Yb)_N$ = 6.17) of the melt inclusions are nearly identical to those of the whole rocks (Ti/Y = 650; $(La/Yb)_N$ = 6.63).

### 4.3. Pb Isotope Compositions of Melt Inclusions

The Lijiang melt inclusions (age-corrected to 260 Ma) exhibit a wide range of Pb isotopic compositions (Figure 4). The $^{208}Pb/^{206}Pb$ and $^{207}Pb/^{206}Pb$ ratios of the melt inclusions in the Lijiang picrites vary from 2.015 to 2.201 and from 0.812 to 0.882, respectively. They are strongly correlated, continuous, and cover the Pb isotopic range from FOZO to EM1 (Figure 4). The compositional range of Lijiang olivine-hosted melt
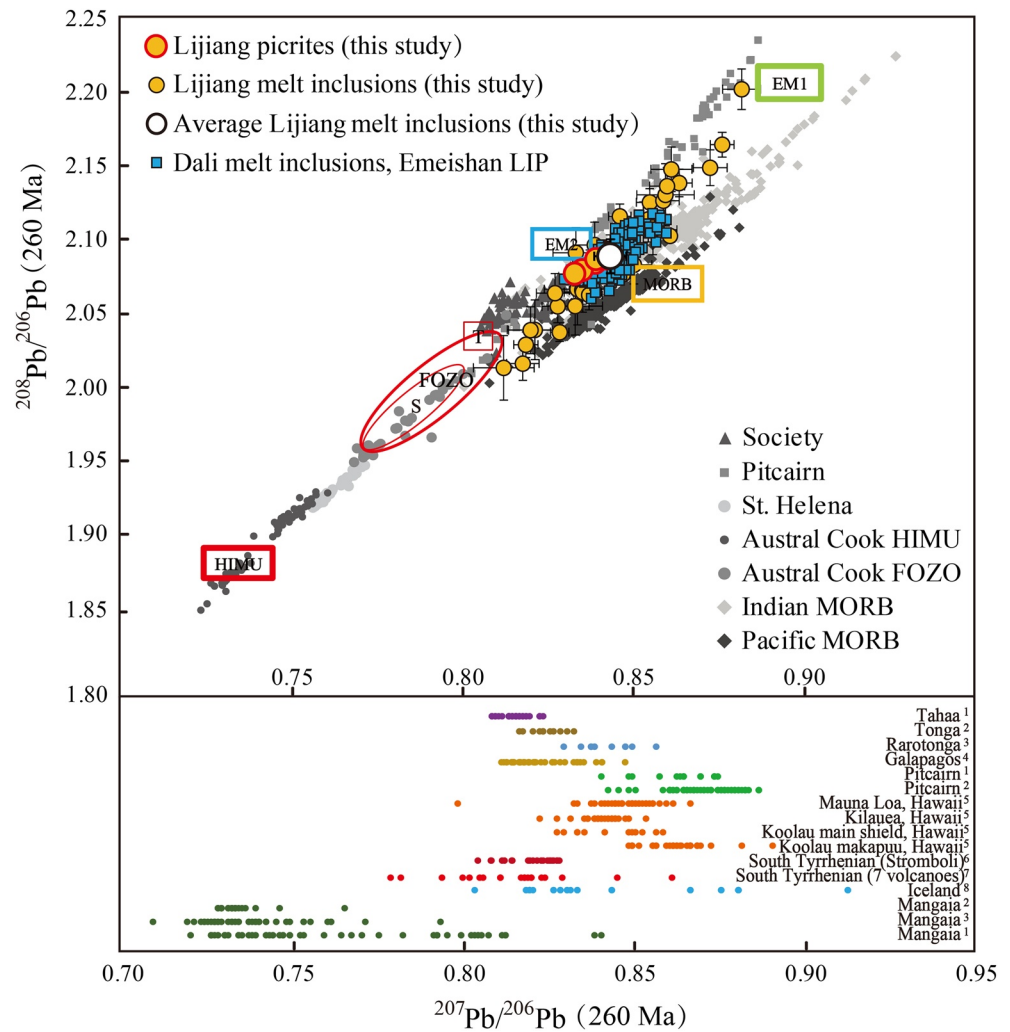
**Figure 4.** $^{208}Pb/^{206}Pb$ versus $^{207}Pb/^{206}Pb$ diagram for Lijiang melt inclusions and host picrites. The compositions of Dali melt inclusions (from Ren et al., 2017; L. Zhang et al., 2019) and typical OIB and MORB (from Stracke, 2012) are also plotted for comparison. The field delimited by the ellipse marked "S" is the FOZO composition from Stracke et al. (2005). The square marked "T" is the FOZO component reported by Hart and Jackson (2014), which is the extreme Pb isotope composition of the Ta'U basalts from Samoa ($^{208}Pb/^{206}Pb = 0.80649$; $^{207}Pb/^{206}Pb = 2.03884$). The variation ranges of Pb isotope compositions of melt inclusions from other studies are also shown. The dotted lines show the compositional ranges of $^{207}Pb/^{206}Pb$ from the melt inclusions in each area. The sample sources are shown at the end of each dotted line, and the numbered labels are references: 1. Saal et al., 2005; 2. Rose-Koga et al., 2017; 3. Paul et al., 2011; 4. Yurimoto et al., 2004; 5. Peterson et al., 2014; 6. Sakyi et al., 2012; 7. Borisova et al., 2014; 8. Schiavi et al., 2012; 9. Rose-Koga et al., 2012; 10. Maclennan, 2008a. Error bars indicate 1 standard error (1SE).

inclusions (within picrites from one sampling point) span almost half of the Pb isotope variability previously reported in OIBs worldwide and are wider than most of the Pb isotopic compositions for olivine-hosted melt inclusions previously reported (Figure 4).

## 5. Discussion

### 5.1. Controls on the Variations in the Compositions of Melt Inclusions

Unlike the homogeneous compositions of the Lijiang picrites themselves, melt inclusions in these picrites have a wide range of major and trace element and Pb isotopic compositions. Although many of the continental flood basalts are thought to be associated with mantle plumes and are therefore of high importance to investigations of the Earth's mantle, they are usually evolved and have been contaminated by crustal
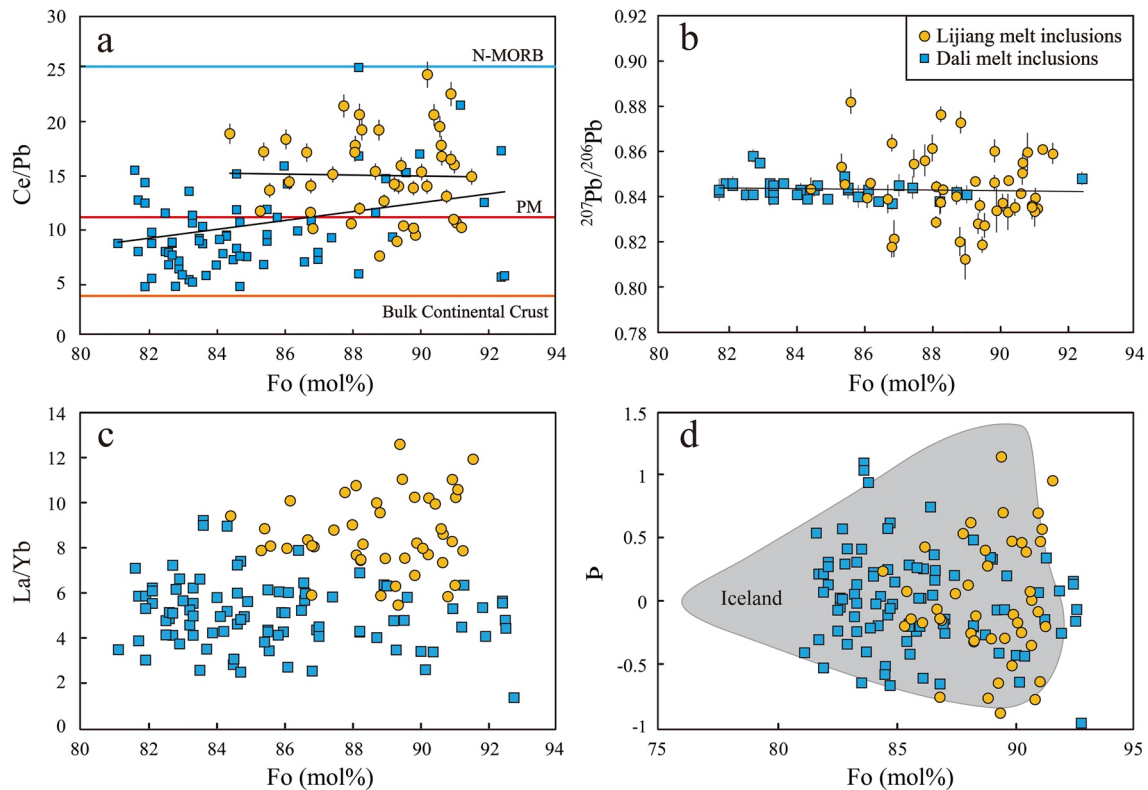
**Figure 5.** Plots of (a) Ce/Pb, and (b) $^{208}$Pb/$^{206}$Pb, (c) La/Yb, and (d) Þ of Lijiang and Dali melt inclusions versus Fo content of host olivines. Data for Dali melt inclusions are from L. Zhang et al. (2019) and J. Liu et al. (2017) (a and b) The black lines are linear regression lines, and there are no correlations shown between Lijiang melt inclusion compositions with Fo value of the host olivines. The composition of bulk continental crust is from Rudnick and Gao (2003); the N-MORB composition is from Sun and McDonough (1989); the PM is primitive mantle and composition is from McDonough and Sun (1995). The error bars with $^{207}$Pb/$^{206}$Pb data indicate 1 standard error (1SE), and error bars with trace element ratios indicate 2 standard error (2SE) (c and d) Shows the trace element variability of melt inclusions in the Lijiang and Dali picrites. The parameter Þ is described in detail in Maclennan (2008b). Given that different eruptions have different compositional fields and average compositions. Using the parameter Þ can therefore possible to compare the variability and mixing processes between different eruptions with olivine-hosted melt inclusion compositions. Icelandic melt inclusion compositions are from the compilation of Maclennan (2008b). The trace element compositions of Lijiang and Dali melt inclusions both exhibit large variability comparable to that of Icelandic basalts.

materials while ascending through the thick continental crust (White, 2010). Thus, verifying the influence of possible shallow assimilation processes on the observed variation in the composition of melt inclusions is necessary before using these compositions to trace their mantle sources. The variations in Ce/Pb and $^{207}$Pb/$^{206}$Pb ratios are sensitive to crustal assimilation. In Figures 5a and 5b, the Ce/Pb and $^{207}$Pb/$^{206}$Pb for the Lijiang melt inclusions do not show correlation with the Fo content of host olivines. Thus, the observed compositional variations in the Lijiang melt inclusions are not a result of crustal contamination during the ascent of magma to the surface.

Another issue that needs to be considered is the relationship between Lijiang melt inclusions and picrites; that is, whether these melt inclusions and picrites can indicate the same source characteristics. The major element compositions of the Lijiang picrites have been influenced by the accumulation of olivine (Figure S1); thus, we present here the compositional trends that gradually subtract olivine from the average whole-rock composition (Figure 2a). The major element compositions of the melt inclusions plot along the trends of olivine accumulation, but exhibit considerable variation at a given MgO content (Figure 2a). Besides that, we also calculated the major and trace element components of the primary magma using the Lijiang melt inclusion compositions (results in Table S8 and S9). Our calculation was made using the "Reverse Crystallization" module in the PETROLOG 3 software (Danyushevsky & Plechov, 2011) and using the olivine-melt model of Ford et al. (1983). The initial oxidation state was set to $Fe^{2+}/Fe^{3+} = 9.0$ and olivine was added in 0.1% increments until the composition of melts was equilibrated with the most forsteritic olivine found in Lijiang area (Fo$_{91.6}$, from this study). We also normalize the whole-rock compositions to
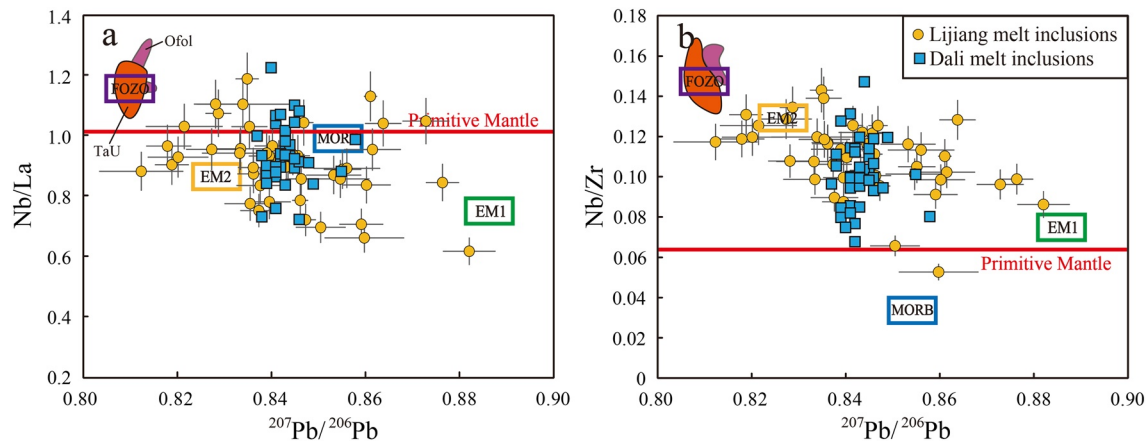
**Figure 6.** Plots of (a) Nb/La and (b) Nb/Zr versus $^{207}Pb/^{206}Pb$ for Lijiang and Dali melt inclusions. The $^{207}Pb/^{206}Pb$ ratios of EM1, EM2, and MORB are from Saal et al. (2005). The Nb/La, Nb/Zr ratios of the EM1, EM2, and MORB end-members are from Weaver (1991). The $^{207}Pb/^{206}Pb$ and the incompatible trace element ratios of Ta'U and Ofol lavas (Hart & Jackson, 2014) are plotted here to indicate the FOZO end-member. The compositions of Dali melt inclusions are from L. Zhang et al. (2019). Although the trace element ratios of melt inclusions have large variability, they have weak correlations with $^{207}Pb/^{206}Pb$ and generally correspond to the FOZO-EM1 trend. The error bars for $^{207}Pb/^{206}Pb$ data indicate 1 standard error (1SE), and error bars for trace element ratios indicate 2 standard error (2SE). EM1, enriched mantle 1.

MgO = 18.64 wt.% (the highest MgO of the primary magma compositions of the Lijiang picrites in this study) by subtracting the average olivine from the whole rock. For most of the elements, the average trace element compositions of the Lijiang melt inclusions resemble to those of the whole rocks when both are normalized to similar MgO content (Figure 3b). Similarly, the average Pb isotopic compositions of the melt inclusions ($^{208}Pb/^{206}Pb$ = 2.089, $^{207}Pb/^{206}Pb$ = 0.844, white dot in Figure 4) are basically equivalent to those of their host whole rocks.

Collectively, although the melt inclusions have wide ranges of major and trace element and Pb isotopic compositions, the average composition of the melt inclusions is approximately equivalent to their whole-rock compositions. This feature is a ubiquitous phenomenon in melt inclusions studies (e.g., Kamenetsky et al., 2012; Kent et al., 2002; Nielsen et al., 1995; Paul, 2011; Ren et al., 2017; Valer et al., 2017). A wide range of melt compositions are produced during mantle melting, much wider than the whole-rock compositions we observed. The compositional heterogeneity of mantle melts is quickly destroyed by subsequent magma ascent and convective stirring, which eventually leads to a mixture of whole-rock components. Higher Fo olivines that form at an early stage of crystallization have the potential to capture inclusions of unmixed or less-mixed parental melts (Maclennan, 2008b; Ren et al., 2005; Sobolev et al., 2011; Sobolev & Shimizu, 1993; Sours-Page et al., 1999, 2002). Therefore, the melt inclusion components in the Lijiang picrites represent imperfectly mixed melts that were present during the early stage of magma evolution. In the following discussion, both the whole-rock and melt inclusion compositions are used to study the nature of the mantle sources: the whole-rock compositions reflect the "average" composition of mantle-derived melts that formed the Lijiang picrites, while the melt inclusions effectively record the small-scale compositional heterogeneity of the mantle melts.

## 5.2. The Source Characteristics of the Lijiang Picrites

### 5.2.1. The Two End-Members of Lijiang Sources

In Figure 6, the $^{207}Pb/^{206}Pb$ (as well as $^{208}Pb/^{206}Pb$) ratios of Lijiang melt inclusions show weak negative correlations with Nb/La and Nb/Zr, possibly suggesting mixing between a low $^{207}Pb/^{206}Pb$ end-member and a high $^{207}Pb/^{206}Pb$ end-member. In the $^{208}Pb/^{206}Pb$ versus $^{207}Pb/^{206}Pb$ plot (Figure 4), the Lijiang melt inclusions form a well-defined array and can be explained as mixtures of the FOZO and EM1 mantle components. This explanation also applies to the correlation of Nb/La and Nb/Zr with $^{207}Pb/^{206}Pb$ for the Lijiang melt inclusions (Figure 6). In the Nb/Y versus Zr/Y diagram (Figure 7), the Lijiang melt inclusions plot generally within the Iceland mantle array and are distinct from MORB in composition (Fitton et al., 1997, 2003).
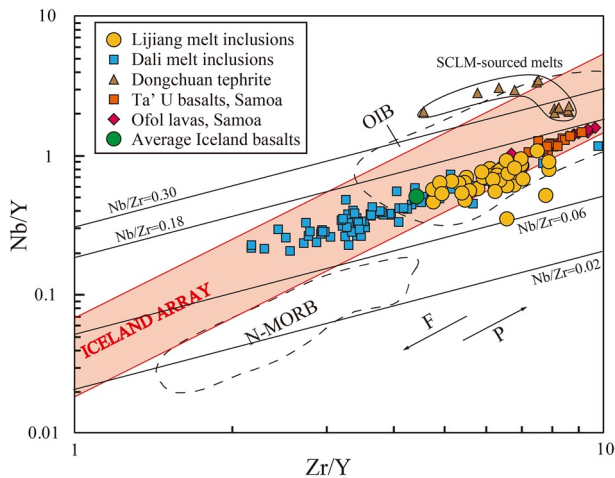
**Figure 7.** Nb/Y versus Zr/Y for Lijiang and Dali melt inclusions. This plot was proposed by Fitton et al. (1997). The green dot is the average Icelandic basalt from Fitton et al. (2003). F and P arrows indicate the approximate effects of increasing degree of melting and pressure, respectively. The Iceland array is considered to reflect the compositional field of the plumes mantle in general (Fitton et al., 1997, 2003). Lijiang and Dali melt inclusions generally plot within the Iceland array and differ from the composition of N-MORB. The Dongchuan tephrites, which are considered to be derived from the melting of the subcontinental lithospheric mantle heated by the Emeishan mantle plume, are plotted for comparison (Song et al., 2008). The data sources for Dali melt inclusions and Ta'U & Ofol lavas are the same as in Figures 3 and 6, respectively.

The Lijiang melt inclusion compositions are linearly correlated with the FOZO-affinity lavas from Ta'U and Ofol (Hart & Jackson, 2014). Furthermore, in the primitive mantle-normalized trace element diagram, the patterns of Lijiang picrites are subparallel to that of the Ta'U basalt, whose source is considered to represent the FOZO end-member (Hart & Jackson, 2014; Figure 3a).

We consider that the low $^{207}Pb/^{206}Pb$ and high Nb/La and Nb/Zr mantle end-member in the source of the Lijiang picrites is FOZO-like, which is generally considered to represent material from the lower mantle and may be a mixture of mantle plumes originating from the deep mantle (Hart et al., 1992; Hauri et al., 1994; Lee et al., 2010). This end-member component has also been observed in the Dali picrites (Ren et al., 2017) and may represent a ubiquitous "matrix" component in the mantle source of the Emeishan LIP.

In comparison, the high $^{207}Pb/^{206}Pb$ component is typified by low Nb/La and Nb/Zr. In Figure 7, some of the melt inclusions exhibit lower Nb contents, which trend toward the lower bound of the Iceland array. Given that the melt inclusions with lower Nb/Zr also have unradiogenic Pb (Figure 6b), these melt inclusions with lower Nb/Zr (plotting below the Iceland array) are not the result of higher degrees of melting of MORB but rather suggest the contribution of crustal-like components or derived sediments. These melt inclusions are characterized by extremely unradiogenic Pb, which are typically observed in EM1 (Figures 4 and 6). Combining the trace element and isotope characteristics of the melt inclusions, we consider that this end-member may reflect the involvement of a recycled component in the source of the Lijiang picrites. Below, we discuss the nature of the recycled component that forms the EM1-like signature in Lijiang melt inclusions.

### 5.2.2. The Origin of EM1 Signatures in Lijiang Melt Inclusions

The primitive mantle normalized trace element patterns of the Lijiang melt inclusions shows that some melt inclusions are evidently depleted in Nb and Ta compared to adjacent elements (Rb, Ba, Th, U, La, and Ce), and have subdued negative Pb anomalies, and some of them even have slightly positive Pb anomalies (Figure 8). Given that the melt inclusions with crustal trace element characteristics also have higher $^{207}Pb/^{206}Pb$ ratios (Figure 6), this crustal-derived component is considered to be responsible for the EM1-like component in the mantle source of the Lijiang picrites.

The mantle source of EM1 is generally characterized by low $^{206}Pb/^{204}Pb$ and $^{143}Nd/^{144}Nd$ and high $^{87}Sr/^{86}Sr$ ratios. The prevailing views regarding the origin of the EM1 signature generally ascribe it to the involvement of: 1) lower continental crust (Escrig et al., 2004; Frey et al., 2002; Hanan et al., 2004; Willbold & Stracke, 2006, 2010), 2) delaminated subcontinental lithospheric mantle (Geldmacher et al., 2008; Gibson et al., 2005; Turner et al., 2017), 3) carbonated mantle (Carlson, 1995; X. J. Wang et al., 2018), or 4) oceanic crust with a small amount of pelagic sediment (Chauvel et al., 1992; Eisele et al., 2002; Garapic et al., 2015; Lassiter & Hauri, 1998; Weaver, 1991).

The lower continental crust is characterized by high Th/U and low (Th, U)/Pb ratios and positive Ba anomalies (Figure 8; Rudnick & Fountain, 1995; Rudnick & Gao, 2003), which could develop high $^{208}Pb^*/^{206}Pb^*$, low $^{206}Pb/^{204}Pb$, and high Ba/Nb ratios (Hanan et al., 2004; Willbold & Stracke, 2006). Thus, many studies have proposed that the origin of EM1 basalts is related to recycling of the lower continental crust, and this model has been used to successfully explain the compositional characteristics of EM1 in many cases (Escrig et al., 2004; Hanan et al., 2004; Willbold & Stracke, 2006, 2010). The trace element compositions of the lower continental crust are clearly different from those of the upper continental crust and derived sediments (Figure 6). The most obvious difference is that the lower continental crust shows no Th enrichment, does not exhibit marked Nb depletion, and is characterized by higher Nb/Th and lower Th/La ratios compared with
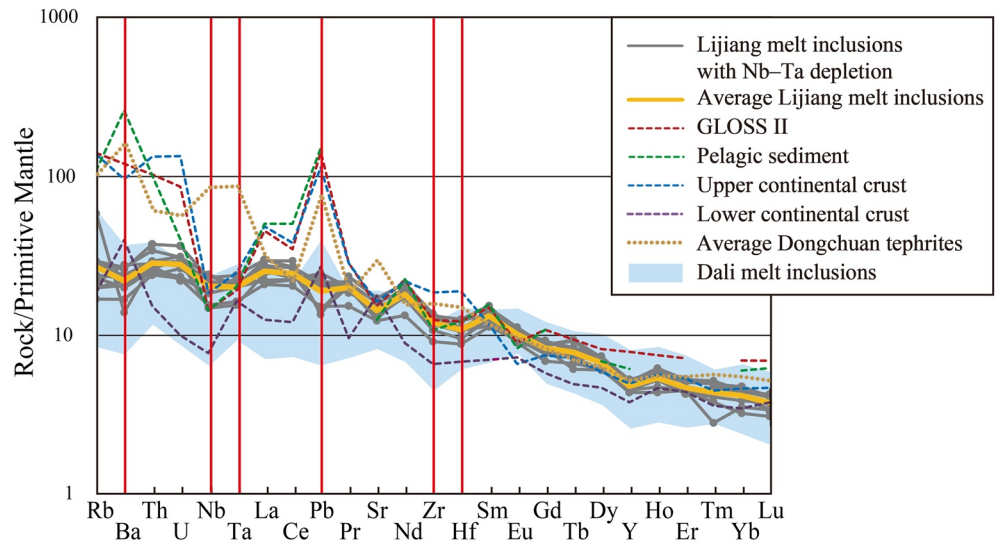
**Figure 8.** Trace element patterns of the melt inclusions with Nb–Ta depletion. These melt inclusions were selected with the constraints of low Nb/Th and Ta/La. Upper continental crust (blue dashed line), lower continental crust (purple dashed line), global subducting sediments II (GLOSS II, red dashed line), pelagic sediments (green dashed line), and the average composition of Dongchuan tephrites (yellow dotted line) are also plotted for comparison. Data for the upper and lower continental crust are from Rudnick and Gao (2003), the primitive mantle is from McDonough and Sun (1995), GLOSS II is from Plank (2014), and pelagic sediment shown is the pelagic sediment composition from Ontong Java Ref. Site 261 reported by Plank and Langmuir (1998), which has representative characteristics of high Ba, high Th/U, low U/Pb ratios. The data source of Dongchuan tephrites are from Song et al. (2008).

upper continental crust or sediments (Frey et al., 2002; Plank, 2005). Therefore, the addition of the lower continental crust materials would not substantially lower the Nb/Th ratio but would significantly increase the Ba/Th ratio. The Lijiang melt inclusions with crustal signatures have evidently low Nb/Th (4.3–7.0) and Ba/Nb (9.4–11.8) ratios, a feature that is inconsistent with the involvement of lower continental crust (Figures 9a and 9b). Therefore, the involvement of melts from the lower continental crust is not compatible with the compositional characteristics of Lijiang melt inclusions.

The SCLM and carbonated mantle are unlikely the components to have formed the EM1 signature in Lijiang melt inclusions. Many SCLM xenoliths have isotopic compositions similar to those of EM1 and are therefore candidates for the genesis of EM1 basalt (e.g., Gibson et al., 2005; McKenzie and O'Nions, 1983). Although no mantle xenoliths have been found in the Emeishan LIP, the Dongchuan tephrites have been deemed as being derived from mantle plume triggered melting of a metasomatized SCLM component under the Emeishan LIP (Song et al., 2008). The Dongchuan tephrites are located in the eastern part of the Emeishan LIP and show high Nb/La (2.0–3.9) and $^{87}Sr/^{86}Sr_{(i)}$ (0.7069–0.7088) ratios and extremely low $\varepsilon_{Nd(t)}$ values (−10.6–−11.1; Song et al., 2008). However, the Dongchuan tephrites exhibit positive Ba, Sr, and Nb–Ta anomalies, and extremely high Nb/La values in the primitive mantle-normalized trace element diagram, which differs from the recycled component signature revealed by Lijiang melt inclusions (Figure 8). Moreover, the compositional trends of Lijiang melt inclusions in an Nb/Y–Zr/Y diagram do not support the involvement of melts similar to those of the Dongchuan tephrites, which show high Nb/Zr ratios (Figure 7). In addition, given the highly enriched Sr–Nd isotope compositions of the Dongchuan tephrites, a small amount of SCLM involved in the source of the Lijiang picrites would substantially change the Sr–Nd isotope signature of the Lijiang picrites, which is inconsistent with the depleted Sr–Nd isotope characteristics of the Lijiang picrites (Figure S4).

A carbonatitic origin for the Lijiang picrites is unlikely because the carbonated mantle has been considered a possible source for alkalic basalts (e.g., Dasgupta et al., 2007; Hirose, 1997; Schmidt & Weidendorfer, 2018), whereas the Lijiang picrites are tholeiitic. Moreover, a Mg isotope study of basalts from the Emeishan LIP has shown that $\delta^{26}Mg$ ranges from −0.35‰ to −0.19‰, which is consistent with the mantle average (−0.25 ± 0.07‰; Teng et al., 2010), which does not favor significant involvement of a carbonatitic
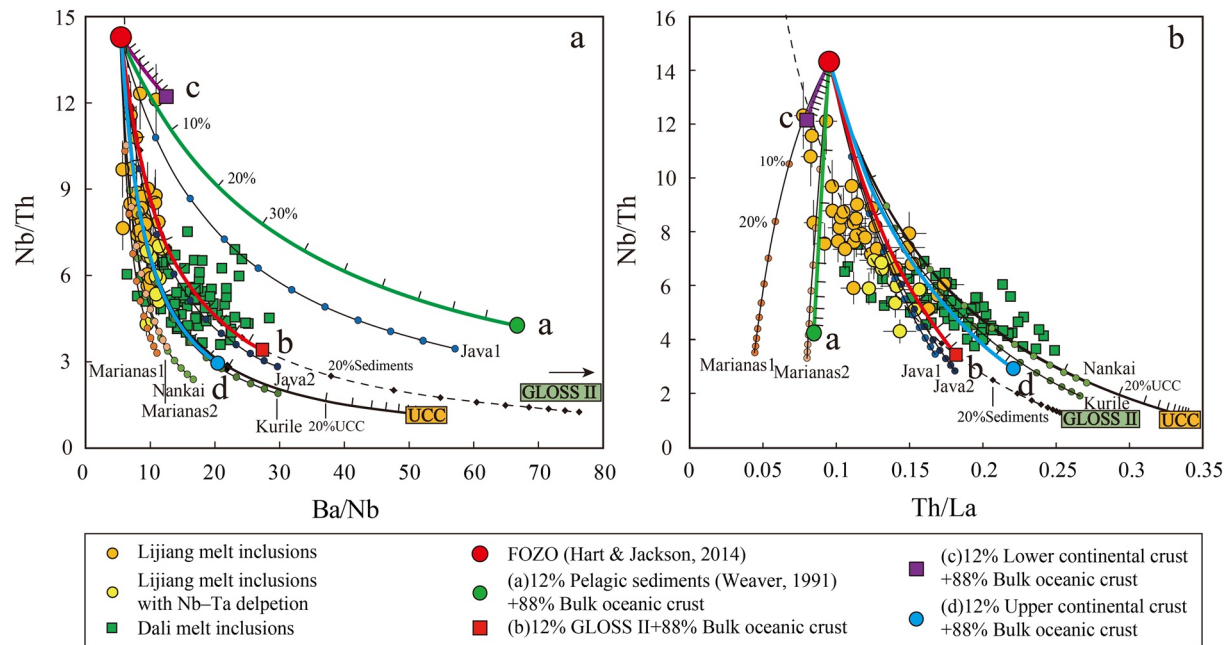
**Figure 9.** (a) Nb/Th versus Ba/Nb and (b) Nb/Th versus Th/La for Lijiang melt inclusions. The yellow circles are Lijiang melt inclusion compositions, and the light yellow circles are melt inclusions with Nb–Ta depletion, corresponding to the melt inclusions in Figure 8. The solid colored curves (red, green, blue, and purple) illustrate mixing lines between FOZO mantle and recycled materials. The recycled material components are set to (a) 12% pelagic sediments (composition from Weaver, 1991) + 88% bulk oceanic crust (green circle), (b) 12% GLOSS II (Plank, 2014) + 88% bulk oceanic crust (red square), (c) 12% lower continental crust (Rudnick & Gao, 2003) + 88% bulk oceanic crust (purple square), and (d) 12% upper continental crust (Rudnick & Gao, 2003) + 88% bulk oceanic crust (blue circle). The tick mark on the mixing curve indicate 10% increments of the recycled materials in the mixture. The solid black curves with small dots illustrate mixing lines between FOZO mantle and recycled materials (12% sediments + 88% bulk oceanic crust), in which recycled sediments are pelagic sediments from different trenches. The recycled sediments used in modeling are pelagic clays from Plank and Langmuir (1998), and the drill sites for these pelagic sediments are as follows: Java1-DSDP 221, Java2-DSDP 261, Marianas1-ODP 801, Marianas2-ODP 800, Nankai-ODP808, and Kurile-DSDP 581. The black dashed line is the mixing line between recycled bulk oceanic crust and subduction-modified GLOSS II. The solid black curve with UCC illustrates mixing lines between the FOZO mantle and upper continental crust. The big red circle is the estimated source composition of Ta'U basalts in Samoa from Hart and Jackson (2014) (Ba = 13.3 ppm, Th = 0.17 ppm, Nb = 2.44 ppm, La = 1.79 ppm), which represents the composition of FOZO mantle. The recycled bulk oceanic crust and all recycled sediments used in the modeling are compositions after subduction modification (Johnson & Plank, 1999; Plank & Langmuir, 1998). The data source for bulk oceanic crust is from Stracke et al. (2003), and is composed of 25% N-MORB (Hofmann, 1988) + 25% altered MORB (Staudigel et al., 1996) + 50% gabbro (Hart et al., 1999). The error bars indicate 2 standard error (2SE).

component in the Emeishan LIP (Tian et al., 2017). A Zn isotope study has also shown that the $\delta^{66}Zn$ values of Emeishan picrites and basalts ranges from 0.24‰ to 0.34‰, which is not compatible with the presence of carbonatitic components in the sources of the Emeishan LIP, but may be the joint consequence of the addition of recycled oceanic crust and mantle melting (C. Yang & Liu, 2019).

Recycled oceanic crust with pelagic sediment is one of the main favored models for the origin of the EM1 signature of basalts (e.g., Chauvel et al., 1992; Eisele et al., 2002; Garapic et al., 2015; Hauri et al., 1996; Stracke, 2003; Weaver, 1991; Weaver et al., 1986; Woodhead et al., 1993). Pelagic sediments are considered to be typically enriched in Ba and to have high Th/U ratios (Othman et al., 1989; Weaver, 1991). Furthermore, pelagic sediments commonly have low Th/La ratios (Elliott et al., 2007; Zhao et al., 2019) and are considered deficient in zircon, which would lead to radiogenic Hf at a given $\varepsilon_{Nd}$ (Bayon et al., 2009; Blichert-Toft et al., 1999; Vervoort et al., 2011). In contrast, the Lijiang melt inclusions are depleted in Ba relative to other large-ion lithophile elements (LILEs) (Figures 2 and 8), and the Ba/Nb and Ba/Th ratios of the Lijiang melt inclusions are relatively low (Ba/Nb = 5.7–11.8; Ba/Th = 41.3–140.6) compared with those of typical OIB (Figure S6). In addition, the Lijiang melt inclusions generally trend toward a composition with relatively higher Th/La ratios (Figure 9b), and, suggesting that no Nd–Hf isotope decoupling has occurred in the compositions of the Lijiang picrites (Figure S4). For these reasons, the typical pelagic sediments (e.g., Weaver, 1991) do not appear to be the source of EM1 signatures in the Lijiang melt inclusions.

With the increasing number of trenches and sediments assessed, researchers have realized that pelagic sediments have highly diverse compositions (Plank, 2014; Plank & Langmuir, 1998; Vervoort et al., 2011). Some pelagic sediments (e.g., Nankai sediments, Figures 9a and 9b) also have trace element compositions that can explain the compositional character of the Lijiang melt inclusions. Plank and Langmuir (1998) and Plank (2014) proposed that the chemical components of sediments are dominated by lithology and that the term "pelagic" would be better associated with sedimentological factors to obtain a more comprehensive understanding of the chemical composition of subducting sediments. For instance, the Ba concentration of sediments is controlled chiefly by biogenic phases and hydrothermal fluids, and the Th concentration is related to fish debris and Fe–Mn oxides. The low Ba, intermediate Th/U, and high Th/La values shown by the Lijiang melt inclusions and the lack of $\varepsilon_{Nd}$–$\varepsilon_{Hf}$ decoupling found in the Lijiang picrites may reflect that the sediments in the source of Lijiang picrites lack products of biological activity and Fe–Mn oxides but contain a dominant amount of terrigenous material. Compared to "pelagic" sediments, we suggest that a component similar to GLOSS II (Global Subducting Sediments II; Plank, 2014) may be appropriate for representing the recycled sediments in the source of the Lijiang picrites. GLOSS II has low Ba/Nb and Ba/La, high Th/La, and intermediate Th/U ratios, characteristics that are compatible with the trace element characteristics shown by the Lijiang melt inclusions. In Figure 9, the trace element contents of the Lijiang melt inclusions are more consistent with the mixing array of recycled oceanic crust + GLOSS II with FOZO mantle.

It should be mentioned that, recycled materials may undergo modifications such as fluid reworking and even partial melting during the process of recycling into the mantle (Class & le Roex, 2008; Jackson et al., 2007; Johnson & Plank, 1999), and recycled components may accumulate and mix in the deep mantle before returning to the shallower mantle (Weaver, 1991; Workman et al., 2004). In addition, the origins of EM1 are multifarious, and there may be many subclasses of "EM1" that are formed principally by compositionally heterogeneous recycled components and/or varied geological processes. Our model is proposed combination of the trace element and Pb isotope characteristics of the Lijiang picrites and melt inclusions, and we think that the involvement of a GLOSS II-like component can account for the high $^{207}Pb/^{206}Pb$ end-member in the Lijiang sources. Furthermore, although the trace element and isotopic compositions of subduction sediments are similar to those of the upper continental crust in many ways, they are clearly different in some respects. For example, GLOSS II exhibits higher Th/U ratios [GLOSS II = 4.11 (Plank, 2014); UCC = 3.89 (Rudnick & Gao, 2003)] and lower U/Pb ratios [GLOSS II = 0.08; UCC = 0.16] than those of UCC. Therefore, the time-integrated evolution of global subduction sediments should result in comparative higher $^{208}Pb/^{206}Pb$ and lower $^{206}Pb/^{204}Pb$ ratios, which are consistent with EM1 characteristics. In addition, according to the experiments on the dehydration and melting of sediments, Pb is less mobile relative to U and Th during sediment subduction (Johnson & Plank, 1999), which also suppresses the U/Pb ratio. Furthermore, due to mineral selectivity during transportation, subduction sediments tend to have lower $^{87}Sr/^{86}Sr$ compared with upper continental crust [GLOSS II $^{87}Sr/^{86}Sr$ = 0.71236 (Plank, 2014); NACS $^{87}Sr/^{86}Sr$ = 0.7313 (McCulloch & Wasserburg, 1978)]. Jackson et al. (2007) showed that a source involving old recycled upper continental crust is compatible with the ultra-enriched EM2 type lavas with extremely high $^{87}Sr/^{86}Sr$ ratios in Samoa, but excluded global subduction sediments as a potential component because of their comparative lower $^{87}Sr/^{86}Sr$ ratios. Therefore, considering the above-mentioned lines of evidence, old recycled GLOSS II-like sediment + oceanic crust can also exhibit the isotopic characteristics of EM1.

### 5.2.3. The Isotope Modeling and Recycling Age

Previous studies have shown that the recycling age of recycled components can vary greatly. The younger limit of the recycling age is traditionally considered to be 0.5 Ga (e.g., Peterson et al., 2014). Some studies have also found Archean recycled materials in the mantle (Ashwal et al., 2017; Cabral et al., 2013; Delavault et al., 2016). In the following discussion, we simulate the variation in isotopes in recycled components as a function of the recycling age and the proportion of sediments in the source.

We modeled the composition of the mantle beneath Lijiang, which is plume mantle with recycled oceanic crust and sediments. We assume the plume mantle is composed of FOZO (Hart & Jackson, 2014) and that the recycled components consist of bulk oceanic crust (Stracke, 2003) + GLOSS II (Plank, 2014), as discussed above. The isotopic composition of the recycled component was calculated using the spreadsheet "basalt+sediment recycling.xls" formulated by Stracke (2003), which can calculate the isotopic evolution of the ancient recycled basalt and sediment. Figure 10 shows the isotopic compositions of the recycled com-
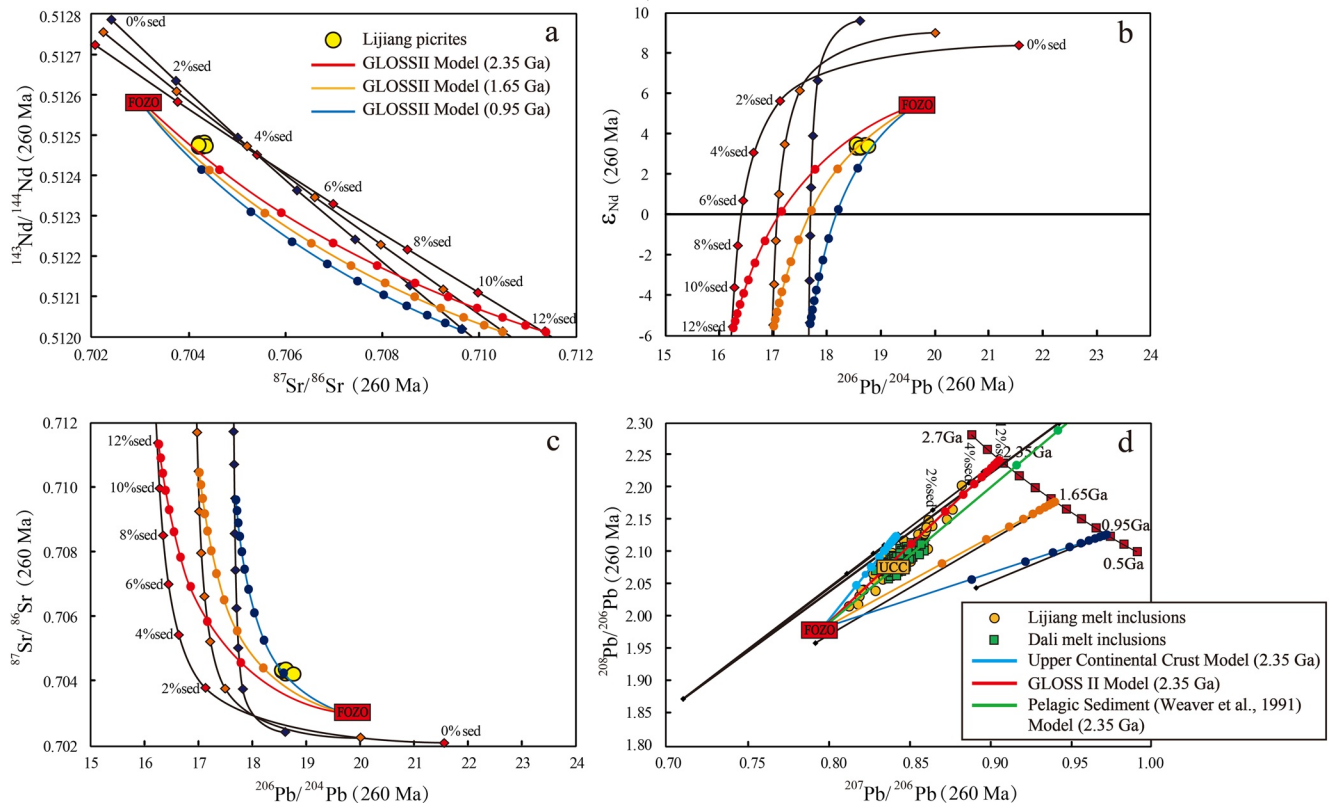
**Figure 10.** Evolution of the recycled component in the (a) $^{143}Nd/^{144}Nd$–$^{87}Sr/^{86}Sr$, (b) $\varepsilon_{Nd}$–$^{206}Pb/^{204}Pb$, (c) $^{87}Sr/^{86}Sr$–$^{206}Pb/^{204}Pb$ and (d) $^{208}Pb/^{206}Pb$–$^{207}Pb/^{206}Pb$ diagrams. The modeling is based on the spreadsheet of Stracke et al. (2003). The black lines with diamonds illustrate mixing lines between recycled oceanic crust and GLOSS II. The labeled diamonds are the proportion of recycled sediments in recycled materials. The red, orange, and blue curves with dots represent source mixing between FOZO mantle and recycled components with recycling ages of 2.35, 1.65, and 0.95 Ga, respectively. Dots on the mixing lines indicate 10% increments of recycled components from 0%–100%. The compositons of recycled oceanic crust and sediments are modified follow the models of Plank and Langmuir (1998), Johnson and Plank (1999), respectively. In (d), the black curve with red squares shows the isotopic composition of the recycled component (in 260 Ma) with different recycling age (0.5–2.7 Ga). Each square on the curve indicates a 0.2 Ga increment of recycling age. The modeling results for the case of recycled material composed of upper continental crust + bulk oceanic crust (blue line) and pelagic sediments + bulk oceanic crust (green line) at 2.35 Ga are also shown for comparison. When the sediment fraction is 12% in the recycled component, both the trace element ratios of melt inclusion in Figure 9 and Pb isotope composition of melt inclusions can basically be reproduced by the consistent model. The Pb isotope composition of UCC shown in the figure are from Millot et al. (2004) and age-corrected to 260 Ma. Detailed parameters and data used in the modeling can be found in Table S14.

ponents with different GLOSS II percentage (black lines) and source mixing between FOZO mantle and recycled components (colored lines). The parameters and compositions used in the modeling are supplied in Table S14.

The Pb isotopic compositions of the Lijiang picrites and their melt inclusions plot along the mixing curves of FOZO and recycled component which composed of bulk oceanic crust and subducted sediments. Our calculations show that a mixture of FOZO and a recycled component composed of 88% bulk oceanic crust +12% GLOSS II can produce a source with ideal isotopic characteristics for the Lijiang picrites and melt inclusions. The modeling results also show that the mixing arrays modeled for different recycling ages have similar compositional trends in $^{143}Nd/^{144}Nd$–$^{87}Sr/^{86}Sr$, $\varepsilon_{Nd}$–$^{206}Pb/^{204}Pb$, and $^{87}Sr/^{86}Sr$–$^{206}Pb/^{204}Pb$ plots (Figures 10a, 10b, and 10c). In contrast, the Pb–Th–U isotope system is sensitive to recycling times in the mantle. In the $^{208}Pb/^{206}Pb$–$^{207}Pb/^{206}Pb$ isotope space presented in Figure 10d, we show the effect of different recycling ages on the Pb isotopic composition of the evolved recycled materials. With increasing recycling age, the final recycled component (in 260 Ma) tends to have higher $^{208}Pb/^{206}Pb$ ratios and lower $^{207}Pb/^{206}Pb$ ratios. The compositions of the Lijiang picrites and melt inclusions plot mostly on the mixing curve of FOZO and a recycled component for a recycling age of 2.35 Ga. Although the recycling age cannot be defined precisely due to the dependence of the model results on the selected parameters, the models indicate an old recycling age is necessary. Moreover, given that the formation age of the Emeishan LIP of 260 Ma,

this estimated recycling age is also consistent with the estimation in previous studies that a period of 1–2 Ga is needed for the recycled component in the mantle to evolve into the trace element and isotopic signature of EM1 basalts (Chauvel, 1992; Hofmann, 1997; Hofmann & White, 1982; Weaver, 1991).

### 5.3. Origin of Variably Enriched Magmas in the Emeishan LIP

With the variation in the Ti/Y of the mafic-ultramafic magmatic rocks in the Emeishan LIP, the other aspects of geochemical composition also vary systematically (Hanski et al., 2010; Huang et al., 2014; Ren et al., 2017; Tian et al., 2017; Xiao et al., 2004; Y. G. Xu et al., 2001). The Binchuan picrites (average Ti/Y = 297) and Yongsheng picrites (average Ti/Y = 790) represent two end-member compositions (low-Ti and high-Ti end-member) in the Emeishan LIP (Kamenetsky et al., 2012). The host picrites of the Lijiang melt inclusions and Dali melt inclusions have Ti/Y ratios of 645–654 and 358–409, and can be classified as high-Ti series and low-Ti series, respectively. Whole-rock and melt inclusion compositions show that, the high-Ti magmas have lower $SiO_2$, $Al_2O_3$, and CaO content compared with the low-Ti magmas (Figure 2). High-Ti magmas usually have OIB-like trace element patterns, whereas trace element patterns of low-Ti magmas are highly variable, but have pronounced negative Nb–Ta anomalies (Hanski et al., 2010; Huang et al., 2014; Tian et al., 2017). In addition, the ΣLREE/ΣHREE ratios vary systematically with the Ti/Y ratios of the magmas, which presented as the high-Ti picrites having higher ΣLREE/ΣHREE than those of the low Ti picrites (Figure S3).

In the Emeishan LIP, the major and trace elements combined with Pb isotope compositions have also been reported for the olivine-hosted melt inclusions in the Dali picrites (Hanski et al., 2010; J. Liu et al., 2017; Ren et al., 2017; L. Zhang et al., 2019). Compared with the compositions of the Lijiang melt inclusions, trace element compositions of the Dali melt inclusions show enrichment in Ba, Th, and Pb content and depletion in Nb content (Figure 3a), as well as exhibit higher Ba/Nb and Th/La, and lower Ce/Pb ratios (Figures 5a and 9). However, the Pb isotopic compositions of the Dali melt inclusions are relatively uniform, and lie within the Pb isotope field of the Lijiang melt inclusions, and these two groups of inclusions have similar average Pb isotopic composition (Figures 4 and 5b).

In the Nb/Th–Ba/Nb plot (Figure 9a), the Lijiang and Dali melt inclusions seem to follow the same trend, which can be explained as a higher proportion of recycled components in the source of the Dali melt inclusions or higher fractions of GLOSS II in the recycled material. However, this explanation is inconsistent with the Pb isotopic characteristics of melt inclusions of the Lijiang and Dali picrites. A higher proportion of recycled components or subduction sediments would lead to higher $^{208}Pb/^{206}Pb$ ratios, but the Dali melt inclusions have intermediate Pb isotopic compositions that plot in the middle of the Pb isotope range of the Lijiang melt inclusions. We consider that the differences in trace element and Pb isotope discrepancies between the Lijiang and Dali melt inclusions are direct consequence of crustal contamination. The upper continental crust has Pb isotopic composition similar to those of the Dali melt inclusions (Figure 10d), and the involvement of upper continental crust can also lead to enrichment in Ba and Th and depletion in Nb and Ta, consistent with the trace element characteristics of the Dali melt inclusions (Figures 8 and 9). We also consider that the upper continental crust signature in the Dali melt inclusions is not a recycled crust component that involved into the mantle of Dali picrites through subduction. As the modeled example in Figure 9 (blue curve), due to the effect of subduction modification and the low fraction of the upper continental crust in the recycled component, the melts from a mantle source into which upper continental crust material was recycled through subduction would have far lower Ba/Nb and Th/La ratios than those observed in the Dali melt inclusions.

Other evidences also suggest that the compositions of melt inclusions of the Dali picrites were affected by crustal contamination. The Ce/Pb ratios of Dali melt inclusions generally decrease with decreasing Fo of the host olivine (Figure 5a), which indicates that the Dali melt inclusion compositions might have been affected by crustal contamination. Besides that, mass balance modeling of the trace element compositions of the Dali melt inclusions has shown that 5% crustal contamination is needed to explain the primitive mantle-normalized trace element patterns of the Dali melt inclusions (L. Zhang et al., 2019). Given the evidence for contamination of the magma from which the Dali melt inclusions were formed (Figure 5a), we consider that the contamination by the upper continental crust is more direct, which can explain the discrepancy between the trace element and Pb isotopic compositions of the Lijiang and Dali melt inclusions. However,

it is possible that other components, such as the SCLM, might have been involved in the magma of the Dali picrites, as the crustal contamination may cover the signature of other potential contributions.

In addition to crustal contamination, other aspects of magmatic evolution also have differed between the Lijiang and Dali picrites. In Figures 5c and 5d, the variation in La/Yb and Þ (the normalized deviation of a melt inclusion composition from the average composition of the eruption, which can be used to indicate the variability of trace element contents; see details in Maclennan, 2008b) for the Lijiang melt inclusions reduces with decreasing Fo of the host olivine, while the trace element variability of the Dali melt inclusions does not reduce similar to the Lijiang melt inclusions. Conversely, the variability of the Dali melt inclusions increases slightly with decreasing Fo. It has been proposed that the olivine and clinopyroxene phenocrysts in the Dali picrites were not crystallized from a well-mixed magma chamber, but rather from magma chambers that underwent recharging, tapping, and fractional crystallization (RTX) processes (Y. D. Wu et al., 2018). Consequently, the observed increase in the variability of the trace element with decreasing Fo of olivine for the Dali melt inclusions may reflect the control exerted by these recharging processes. In summary, the Lijiang magmas ascended to the surface relatively directly compared with the Dali magmas, which underwent complex magmatic processes and extensive contamination during prolonged storage in the magmatic plumbing system.

### 5.4. Al-in-ol Temperatures and Mantle Potential Temperature for the Lijiang High-Ti Picrites and Dali Low-Ti Picrites

The mantle $T_p$ of low-Ti and high-Ti magmatism in LIP is an important consideration in the mantle plume model of LIP formation. As yet, there is no consensus regarding whether high-Ti or low-Ti magmas are derive from mantle with higher thermal energy (He et al., 2010; Tao et al., 2015; Xiao et al., 2004; Y. G. Xu et al., 2001; R. Xu et al., 2020; Yu et al., 2020; Z. C. Zhang et al., 2006). Z. C. Zhang et al. (2006) and He et al. (2010) estimated that the $T_p$ of the mantle of the Lijiang picrites was above 1,627°C on the basis of the high MgO content (22.4–22.9 wt.%) inferred for the primary magma of the Lijiang picrites, and considered that the Lijiang picrites are a product of melting of the hot mantle plume head. However, some studies have suggested that the mantle source of low-Ti magmas had higher $T_p$ than that of high-Ti magmas (Tao et al., 2015; Xiao et al., 2004; Y. G. Xu et al., 2001). Using the method of K. D. Putirka et al. (2007), Tao et al. (2015) determined that the $T_p$ values of low-Ti and high-Ti picrites were 1,740°C–1,810°C and 1,510°C–1,610°C, respectively.

Al-in-ol thermometer has been applied to olivines from the Dali picrites in the Emeishan LIP. R. Xu and Liu (2016) and J. Liu et al. (2017) estimated the maximum crystallization temperatures ($T_{crys}$) of the Dali olivines as 1,432°C and 1,460°C, respectively. J. Liu et al. (2017) further calculated $T_p$ using empirical models of peridotite melting (Herzberg & Asimow, 2015), which yielded a maximum estimated $T_p$ of the mantle beneath Dali of 1,499°C. The Al-in-ol thermometry is based on the sensitivity of the partition coefficient of $Al_2O_3$ between olivine and spinel to crystallization temperature. This method does not have the uncertainty that arises from the estimation of the equilibrium melt composition of olivine and the source lithology, and is not substantially influenced by the $H_2O$ content and $fo_2$ of magma (Coogan et al., 2014). We analyzed spinel inclusions and host olivines from the Lijiang and Dali picrites (analytical results are given in Table S10). In this study, the Cr-spinel inclusions in both the Lijiang and Dali picrites are found in olivines with the highest Fo content, suggesting that the onset time of crystallization of Cr-spinel was early and may simultaneous with that of olivine.

The uncertainty associated with measurements of $Al_2O_3$ content in olivine is the main factor affecting the error on the calculated $T_{crys}$. The errors on the calculated Al-in-ol temperature for each pair of ol–spinel composition were calculated by using Monte Carlo simulations (Heinonen et al., 2015; Matthews et al., 2016). For each ol–spinel pair, we simulated 10,000 Al-in-ol temperature results by random selection of pairs of $Al_2O_3$ in olivine and $Al_2O_3$ and $Cr_2O_3$ in spinel from Gaussian distribution defined by analytical $\sigma$ of $Al_2O_3$ of olivine and $Al_2O_3$ and $Cr_2O_3$ of spinel. From these simulations, we obtained a result for the 1SD uncertainty on the simulated Al-in-olivine temperature of 18°C–25°C.

The highest Al-in-olivine temperature yields 1,380°C and 1,433°C for the Lijiang and Dali picrites, respectively (Figure 11), indicating that the initial crystallization temperatures of the Lijiang olivines are slightly
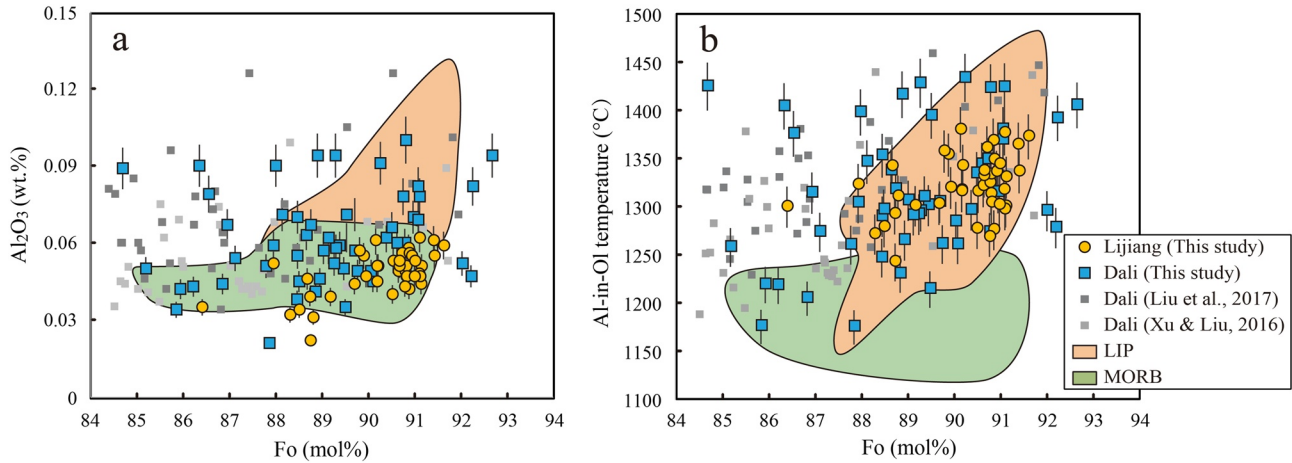
**Figure 11.** Plots of (a) Olivine $Al_2O_3$ and (b) Aluminum-in-olivine temperature versus olivine Fo from the Lijiang and Dali picrites. The compositional fields of LIPs and MORBs are from Coogan et al. (2014). The error bars are analytical error ($2\sigma$) of olivine $Al_2O_3$, and $1\sigma$ errors for the Al-in-ol temperatures. The errors of Fo contents are within symbol sizes. LIPs, large igneous provinces.

lower than those of the Dali olivines. To compare the heat content of the mantle between the Lijiang and Dali picrites, it is necessary to extrapolate the crystallization temperature back to the mantle $T_p$. We followed the back calculation method of K. Putirka (2016), which includes corrections for the latent heat of fusion and the adiabatic cooling. The $T_p$ was calculated based on the following equation (formula 2c in K. Putirka, 2016):

$$T_p = T^{Ol-liq} + F\left(\frac{\Delta H_{fus}}{C_p}\right) - P_1\left(\frac{V\alpha T}{C_p}\right)$$

where $T^{Ol-liq}$ = olivine-liquid equilibration temperature, F = melt fraction, $\Delta H_{fus}$ = Enthalpy of fusion of the mantle, V = molar volume of the mantle, a = coefficient of thermal expansion, $C_p$ = heat capacity of the mantle, $P_1$ = olivine–liquid equilibration pressure, and T = mean temperature along the adiabat between $P_1$ and surface pressure.

The first step of the reverse calculation is to calculate the heat of fusion, which is the heat consumed in the adiabatic system while converting solids to liquids. The melt fraction (F) is an important parameter that affects the heat of fusion. It is commonly considered that high-Ti magmas have a lower degree of melting compared with low-Ti magmas in the Emeishan LIP (e.g., Ren et al., 2017; Shellnutt & Jahn, 2011; C. Y. Wang et al., 2007; R. Xu et al., 2020; Yu et al., 2020; L. Zhang et al., 2019). We estimated the melt fraction of the Lijiang and Dali picrites using the method of K. Putirka (2016) (formula 14b, an empirical equation that calibrates F as a function of the major element composition of primary magma) and the primary magma composition. Results show that the F of the Lijiang and Dali picrites are 14.8% and 29.9%, respectively, which indicates that the mantle of Lijiang has lower melting degree than mantle of Dali. For the parameters of the source lithology, we used the thermal parameters of KG1 (Shorttle et al., 2014) to calculate $T_p$ (the parameters are supplied in Table S15), which are based on the view that the mantle source of the Emeishan LIP is olivine-bearing Si-deficient pyroxenite (Ren et al., 2017). The calculated 1% partial melting of the KG1 source (at 1773 K) would lead to a net temperature decrease of 5.91°C, which is slightly lower than that of peridotite (6.67°C; K. D. Putirka et al., 2007).

The second step of the back calculation is correction for the drop in temperature for adiabatic cooling. To estimate the mantle $T_p$, knowledge of the temperature and pressure of one point on the solid adiabat is required. When back calculating the Al-in-ol temperature to the mantle $T_p$, the pressure corresponding to the depth of crystallization of olivine is considered appropriate as the olivine-liquid equilibration pressure (Matthews et al., 2016). In our calculation, the $P_1$ was set to 1.3 GPa, which is considered to be the crystallization depth of most olivines in the Emeishan picrites (Tao et al., 2015). In addition, the T was set to

1673 K to calculate the adiabatic gradient. The final estimated $T_p$ of the mantle source of the Lijiang and Dali picrites are 1,450°C and 1,592°C, respectively. Although the calculated $T_p$ has an associated uncertainty that arises from factors such as the uncertainty in the source lithology (mineral proportion in the mantle source, e.g., peridotite or pyroxenite), the estimated degree of partial melting (the melt fraction formula of K. Putirka (2016) is based on melting experiments on peridotitic mantle), and the depth of the olivine-liquid equilibration (Heinonen et al., 2015; Jennings et al., 2019; Matthews et al., 2016; K. D. Putirka et al., 2007). However, it can be concluded that the Lijiang high-Ti picrites have both lower Al-in-ol temperatures and lower melting degrees compared with the Dali low-Ti picrites, which indicate that the mantle temperature beneath Lijiang was lower than that beneath Dali.

Our conclusion for $T_p$ beneath Lijiang differs from the previous studies which considered a high $T_p$ ($T_p > 1,627°C$) within the range of the Emeishan LIP (He et al., 2010; Z. C. Zhang et al., 2006). The high $T_p$ obtained by previous studies are based mainly on the high MgO contents of the estimated primary magma, and according to the empirical relationship between primary magma MgO and eruption temperature or source temperature (Albarède, 1992; Herzberg, 2008; Herzberg & O'Hara, 2002; Nisbet et al., 1993). Using these methods, the estimated MgO content of primary magma is decisive for the final $T_p$ results. The Lijiang high-Ti picrites have extremely high MgO contents compared with the picrites from other locations in Emeishan LIP (e.g., average MgO = 27.4 wt.% of the Lijiang high-Ti picrites in this study), while the host picrites of Dali melt inclusions have average MgO = 19.8 wt.% (Figure 2a). The estimated MgO content of the primary magma of the Lijiang high-Ti picrites are also relatively high (22.4–22.9 wt.%) (He et al., 2010; Z. C. Zhang et al., 2006). However, the highest MgO content of melt inclusions (after correction) in the Lijiang high-Ti picrites is significantly lower than that of melt inclusions in the Dali picrites (17.9 and 21.9 wt.%, respectively; Figure 2b), and the calculated MgO contents of the primary magma of the Lijiang high-Ti picrites are significantly lower than those of the Dali low-Ti picrites (Figures 2a and 2b). The method for calculating the primary magma composition we used was adding equilibrium olivines in 0.1% increments until the composition of melts was equilibriated with the most forsteritic olivine found in each area (Lijiang $Fo_{max}$ = 91.6 mol% and Dali $Fo_{max}$ = 93.5 mol%, more parameters are described in Table S8). Thus the Fo content of the most forsteritic olivine is the main factor that dominates the result of our calculation. Using a similar method, Hanski et al. (2010) calculated that the MgO content of the primary magma of the Lijiang high-Ti picrites was lower than that of the Dali picrites. Since the MgO content of primary magma is generally related to the mantle $T_p$, this result is consistent with our conclusion that the mantle $T_p$ beneath Lijiang was lower than that beneath Dali.

In brief, the primary magma compositions of the Lijiang high-Ti picrites estimated by olivine–melt based methods have large uncertainties, which stem from the inversion method used, the choice of the olivine–liquid Mg–Fe exchange distribution coefficient ($K_D$), the $FeO_T$ content of the primary magma, and serious contamination and accumulation of the whole-rock composition. Moreover, the olivine-melt based and empirical thermometers used in the previous studies are based on melting experiments on anhydrous peridotite, and therefore the uncertainties attached to the source lithology and the potential $H_2O$ content of the mantle source are also factors that can lead to difference in estimated $T_p$. If the mantle source was hydrous, the crystallization temperature obtained from the Al-in-ol thermometer would be evidently lower than the olivine-liquid equilibrium temperature estimated by the empirical methods.

### 5.5. A Comprehensive Petrogenetic Model for the Emeishan LIP

The spatial distribution of the basaltic and picritic rocks in the Emeishan LIP generally shows that both low-Ti and high-Ti rocks are found in the inner zone of the LIP, whereas mostly high-Ti rocks are located in the outer zone (Fan et al., 2008; Lai et al., 2012; Xiao et al., 2004; Y. G. Xu et al., 2001, 2004). Moreover, basalts with extremely high Ti/Y in the Emeishan LIP have recently been discovered in western Guangxi (Ti/Y = 761–2018, from X. J. Liu et al., 2016) and are thought to represent the peripheral expression of magmatism of the Emeishan LIP. Another aspect of the distribution of low-Ti and high-Ti magmatic rocks that has been addressed in previous studies is the stratigraphic (temporal) relationship between them. Y. G. Xu et al. (2001) proposed that low-Ti magmatic rocks are confined to the lower parts of stratigraphic columns, whereas high-Ti magmas are located in the upper parts, according to a stratigraphic study of the Binchuan section. However, subsequent studies identified several cases where the low-Ti basalts overlie the

high-Ti basalts (Qi & Zhou, 2008; Shellnutt, 2014; Y. G. Xu et al., 2003). In addition, the distribution of the lithosphere–asthenosphere boundary (LAB) of the Emeishan LIP has been constrained by residual gravity anomaly data (Deng et al., 2014, 2016). The thickness of the lithosphere beneath the Emeishan LIP gradually increases from the inner zone to the outer zone, reaching a maximum depth of ∼160 km in the outer zone (Deng et al., 2016).

On the basis of the geochemical characteristics of the studied melt inclusions and picrites, our new $T_p$ estimation, and the spatial and temporal distributions of magmatism, we consider that the following mantle plume model may systematically explain the evolution of low- and high-Ti magmatism. The high- and low-Ti magmas were both derived from a mantle plume but with differences resulting from spatial–temporal variations of the plume. When the thermal energy of the mantle plume was high, which corresponded to the main stage of magmatism in the axis of the mantle plume, the higher mantle temperature would have led to a higher degree of mantle melting and the resultant production of low-Ti/Y magma. At Dali, which is located in the inner zone of the Emeishan LIP, the higher $T_p$ and thinner lithosphere mutually led to a higher melting degree of the Dali picrites. The extensive contamination of Dali magmas may also be consistent with the early eruption of the axis of the hot mantle plume. Furthermore, the higher $T_p$ would also have led to more extensive convective mixing, resulting in a comparatively homogeneous source for the Dali picrites and melt inclusions.

However, a lower thermal energy of the mantle plume was likely associated with the waning stage of the mantle plume or the periphery of the mantle plume. A lower $T_p$ would have resulted in a lower degree of melting of the plume mantle and the generation of magma with higher Ti/Y ratios. We consider that the Lijiang high-Ti picrites were derived from a waning stage of mantle plume near the plume axis. The lower temperature of the mantle plume mainly led to lower melting degree of the Lijiang high-Ti picrites compared with Dali. Also, compared with the contamination and recharge of magma at Dali during its evolution, the magma at Lijiang appears to have ascended to the surface more directly. The lower temperature for Lijiang magmatism also caused a lower extent of convective mixing, meaning that melts with variable compositions from a heterogeneous mantle did not mix completely and could be captured by melt inclusions enclosed in early formed olivine crystals. In addition, the occurrence of the low-Ti basalts overlying the high-Ti basalts may imply that the variation in thermal energy of the plume mantle might have been characterized by several magma pulses. In summary, on the basis of geochemical and thermodynamic aspects, our study proposes that the Lijiang high-Ti picrites were derived from a mantle source with lower thermal energy, and more generally suggesting that high-Ti magmas in the Emeishan LIP were derived from mantle plume with lower thermal energy.

## 6. Conclusion

The major and trace element and isotope compositions of the Lijiang melt inclusions exhibit greater variability than their host whole-rock compositions, and an enriched component can be recognized. The mantle source of the Lijiang high-Ti picrites was generated by the mixing of a FOZO-like depleted component and an EM1-like enriched component. The trace element and Pb isotopic characteristics of the Lijiang picrites and melt inclusions together suggest that an old recycled GLOSS II-like sediment component may play an important role in the EM1-like composition in the Lijiang sources. Compared to the melt inclusion compositions of the Dali, the Lijiang melt inclusions suggest a lower melting degree and absence of both contamination and magma recharging during magmtic evolution. Moreover, the highly variable Pb isotopic compositions of the Lijiang melt inclusions suggest that the mantle sources of the Lijiang picrites were substantially more heterogeneous relative to the mantle sources of the Dali low-Ti picrites. Furthermore, the Al-in-ol thermometer result shows that the olivines from the Lijiang picrites have lower maximum crystallization temperature than those from the Dali, and the estimated $T_p$ for the Lijiang picrites is also lower. Therefore, we think the Lijiang high-Ti picrites are derived from mantle plume with lower thermal energy, corresponding to the waning stage of the near axis of the mantle plume. We argue that the spatial and temporal variation in the thermal energy of the mantle plume was a key control on the geochemical characteristics of mafic-ultramafic magmatism in the Emeishan LIP.

## Data Availability Statement

Analytical methods and Figures S1–6 can be found in the supporting information S1. All data and parameters reported in this study can be found in Tables S1–15. All supporting information is also available in Figshare (https://doi.org/10.6084/m9.figshare.14445621.v1).

## References

Albarède, F. (1992). How deep do common basaltic magmas form and differentiate? *Journal of Geophysical Research*, *97*(B7), 10997–11009. https://doi.org/10.1029/91JB02927

Ali, J. R., Fitton, J. G., & Herzberg, C. (2010). Emeishan large igneous province (SW China) and the mantle-plume up-doming hypothesis. *Journal of the Geological Society of London*, *167*(5), 953–959. https://doi.org/10.1144/0016-76492009-129

Ali, J. R., Lo, C. H., Thompson, G. M., & Song, X. Y. (2004). Emeishan Basalt Ar–Ar overprint ages define several tectonic events that affected the western Yangtze platform in the Mesozoic and Cenozoic. *Journal of Asian Earth Sciences*, *23*(2), 163–178. https://doi.org/10.1016/S1367-9120(03)00072-5

Anh, T. V., Pang, K. N., Chung, S. L., Lin, H. M., Hoa, T. T., Anh, T. T., & Yang, H. J. (2011). The Song Da magmatic suite revisited: A petrologic, geochemical and Sr–Nd isotopic study on picrites, flood basalts and silicic volcanic rocks. *Journal of Asian Earth Sciences*, *42*(6), 1341–1355. https://doi.org/10.1016/j.jseaes.2011.07.020

Ashwal, L. D., Wiedenbeck, M., & Torsvik, T. H. (2017). Archaean zircons in Miocene oceanic hotspot rocks establish ancient continental crust beneath Mauritius. *Nature Communications*, *8*, 14086. https://doi.org/10.1038/ncomms14086

Bai, Z. J., Zhong, H., Li, C. S., Zhu, W. G., He, D. F., & Qi, L. (2014). Contrasting parental magma compositions for the Hongge and Panzhihua magmatic Fe-Ti-V oxide deposits, Emeishan large igneous province, SW China. *Economic Geology*, *109*(6), 1763–1785. https://doi.org/10.2113/econgeo.109.6.1763

Batanova, V. G., Thompson, J. M., Danyushevsky, L. V., Portnyagin, M. V., Garbe-Schönberg, D., Hauri, E., et al. (2019). New olivine reference material for in situ microanalysis. *Geostandards and Geoanalytical Research*, *43*(3), 453–473. https://doi.org/10.1093/10.1111/ggr.12266

Bayon, G., Burton, K., Soulet, G., Vigier, N., Dennielou, B., Etoubleau, J., et al. (2009). Hf and Nd isotopes in marine sediments: Constraints on global silicate weathering. *Earth and Planetary Science Letters*, *277*(3–4), 318–326. https://doi.org/10.1016/j.epsl.2008.10.028

Blichert-Toft, J., Frey, F. A., & Albarède, F. (1999). Hf isotope evidence for pelagic sediments in the source of Hawaiian basalts. *Science*, *285*(5429), 879–882. https://doi.org/10.1126/science.285.5429.879

Borisova, A. Y., Faure, F., Deloule, E., Grégoire, M., Bejina, F., De Parseval, P., & Devidal, J. L. (2014). Lead isotope signatures of Kerguelen plume-derived olivine-hosted melt inclusions: Constraints on the ocean island basalt petrogenesis. *Lithos*, *198*, 153–171. https://doi.org/10.1016/j.lithos.2014.03.022

Bryan, S. E., & Ernst, R. E. (2008). Revised definition of large igneous provinces (LIPs). *Earth-Science Reviews*, *86*(1–4), 175–202. https://doi.org/10.1016/j.earscirev.2007.08.008

Cabral, R. A., Jackson, M. G., Rose-Koga, E. F., Koga, K. T., Whitehouse, M. J., Antonelli, M. A., et al. (2013). Anomalous sulphur isotopes in plume lavas reveal deep mantle storage of Archaean crust. *Nature*, *496*(7446), 490–493. https://doi.org/10.1038/nature12020

Cao, Y. H., Wang, C. Y., Huang, F., & Zhang, Z. F. (2019). Iron isotope systematics of the Panzhihua mafic layered intrusion associated with giant Fe-Ti Oxide deposit in the Emeishan large igneous province, SW China. *Journal of Geophysical Research: Solid Earth*, *124*, 358–375. https://doi.org/10.1029/2018JB016466

Carlson, R. (1995). Isotopic inferences on the chemical structure of the mantle. *Journal of Geodynamics*, *20*(4), 365–386. https://doi.org/10.1016/0264-3707(95)00027-7

Chauvel, C., Hofmann, A. W., & Vidal, P. (1992). HIMU-EM: The French Polynesian connection. *Earth and Planetary Science Letters*, *110*(1–4), 99–119. https://doi.org/10.1016/0012-821x(92)90042-t

Chen, Y., Xu, Y. G., Xu, T., Si, S. K., Liang, X. F., Tian, X. B., et al. (2015). Magmatic underplating and crustal growth in the Emeishan large igneous province, SW China, revealed by a passive seismic experiment. *Earth and Planetary Science Letters*, *432*, 103–114. https://doi.org/10.1016/j.epsl.2015.09.048

Chung, S. L., & Jahn, B. M. (1995). Plume-lithosphere interaction in generation of the Emeishan flood basalts at the Permian-Triassic boundary. *Geology*, *23*(10), 889–892. https://doi.org/10.1130/0091-7613(1995)023<0889:PLIIGO>2.3.CO;2

Chung, S. L., Jahn, B. M., Genyao, W., Lo, C. H., & Bolin, C. (1998). The Emeishan flood basalt in SW China: A mantle plume initiation model and its connection with continental breakup and mass extinction at the Permian-Triassic boundary. In M. F. J. Flower, S. L. Chung, C. H. Lo, & T. Y. Lee (Eds.), *Mantle dynamics and plate interactions in East Asia, 27* (pp. 47–58). Washington, DC. American Geophysical Union. https://doi.org/10.1029/GD027p0047

Class, C., & le Roex, A. P. (2008). Ce anomalies in Gough Island lavas—trace element characteristics of a recycled sediment component. *Earth and Planetary Science Letters*, *265*(3–4), 475–486.https://doi.org/j.epsl.2007.10.030

Coogan, L., Saunders, A., & Wilson, R. (2014). Aluminum-in-olivine thermometry of primitive basalts: Evidence of an anomalously hot mantle source for large igneous provinces. *Chemical Geology*, *368*, 1–10. https://doi.org/10.1016/j.chemgeo.2014.01.004

Danyushevsky, L. V., Della-Pasqua, F. N., & Sokolov, S. (2000). Re-equilibration of melt inclusions trapped by magnesian olivine phenocrysts from subduction-related magmas: petrological implications. *Contributions to Mineralogy and Petrology*, *138*(1), 68–83. https://doi.org/10.1007/PL00007664

Danyushevsky, L. V., McNeill, A. W., & Sobolev, A. V. (2002). Experimental and petrological studies of melt inclusions in phenocrysts from mantle-derived magmas: An overview of techniques, advantages and complications. *Chemical Geology*, *183*(1–4), 5–24. https://doi.org/10.1016/S0009-2541(01)00369-2

Danyushevsky, L. V., & Plechov, P. (2011). Petrolog3: Integrated software for modeling crystallization processes. *Geochemistry, Geophysics, Geosystems*, *12*(7), Q07021. https://doi.org/10.1029/2011GC003516

Dasgupta, R., Hirschmann, M. M., & Smith, N. D. (2007). Partial melting experiments of peridotite + $CO_2$ at 3 GPa and genesis of alkalic ocean island basalts. *Journal of Petrology*, *48*(11), 2093–2124. https://doi.org/10.1093/petrology/egm053

Delavault, H., Chauvel, C., Thomassot, E., Devey, C. W., & Dazas, B. (2016). Sulfur and lead isotopic evidence of relic Archean sediments in the Pitcairn mantle plume. *Proceedings of the National Academy of Sciences*, *113*(46), 12952–12956. https://doi.org/10.1073/pnas.1523805113

Deng, Y. F., Chen, Y., Wang, P., Essa, K. S., Xu, T., Liang, X. F., & Badal, J. (2016). Magmatic underplating beneath the Emeishan large igneous province (South China) revealed by the COMGRA-ELIP experiment. *Tectonophysics*, *672*, 16–23. https://doi.org/10.1016/j.tecto.2016.01.039

Deng, Y. F., Zhang, Z. J., Mooney, W., Badal, J., Fan, W. M., & Zhong, Q. (2014). Mantle origin of the Emeishan large igneous province (South China) from the analysis of residual gravity anomalies. *Lithos*, *204*, 4–13. https://doi.org/10.1016/j.lithos.2014.02.008

Eisele, J., Sharma, M., Galer, S. J. G., Blichert-Toft, J., Devey, C. W., & Hofmann, A. W. (2002). The role of sediment recycling in EM-1 inferred from Os, Pb, Hf, Nd, Sr isotope and trace element systematics of the Pitcairn hotspot. *Earth and Planetary Science Letters*, *196*(3–4), 197–212. https://doi.org/10.1016/s0012-821x(01)00601-x

Elburg, M., Vroon, P., van der Wagt, B., & Tchalikian, A. (2005). Sr and Pb isotopic composition of five USGS glasses (BHVO-2G, BIR-1G, BCR-2G, TB-1G, NKT-1G). *Chemical Geology*, *223*(4), 196–207. https://doi.org/10.1016/j.chemgeo.2005.07.001

Elliott, T., Blichert-Toft, J., Heumann, A., Koetsier, G., & Forjaz, V. (2007). The origin of enriched mantle beneath São Miguel, Azores. *Geochimica et Cosmochimica Acta*, *71*(1), 219–240. https://doi.org/10.1016/j.gca.2006.07.043

Escrig, S., Capmas, F., Dupré, B., & Allègre, C. (2004). Osmium isotopic constraints on the nature of the DUPAL anomaly from Indian mid-ocean-ridge basalts. *Nature*, *431*(7004), 59–63. https://doi.org/10.1038/nature02904

Fan, W. M., Zhang, C. H., Wang, Y. J., Guo, F., & Peng, T. P. (2008). Geochronology and geochemistry of Permian basalts in western Guangxi Province, Southwest China: Evidence for plume-lithosphere interaction. *Lithos*, *102*(1–2), 218–236. https://doi.org/10.1016/j.lithos.2007.09.019

Fitton, J. G., Saunders, A. D., Kempton, P. D., & Hardarson, B. S. (2003). Does depleted mantle form an intrinsic part of the Iceland plume. *Geochemistry, Geophysics, Geosystems*, *4*(3), 1032. https://doi.org/10.1029/2002GC000424

Fitton, J. G., Saunders, A. D., Norry, M. J., Hardarson, B. S., & Taylor, R. N. (1997). Thermal and chemical structure of the Iceland plume. *Earth and Planetary Science Letters*, *153*(45), 197–208. https://doi.org/10.1016/s0012-821x(97)00170-2

Foley, S. F., Prelevic, D., Rehfeldt, T., & Jacob, D. E. (2013). Minor and trace elements in olivines as probes into early igneous and mantle melting processes. *Earth and Planetary Science Letters*, *363*, 181–191. https://doi.org/10.1016/j.epsl.2012.11.025

Ford, C., Russell, D., Craven, J., & Fisk, M. (1983). Olivine-liquid equilibria: Temperature, pressure and composition dependence of the crystal/liquid cation partition coefficients for Mg, $Fe^{2+}$, Ca and Mn. *Journal of Petrology*, *24*(3), 256–266. https://doi.org/10.1093/petrology/24.3.256

Frey, F. A., Weis, D., Borisova, A. Y., & Xu, G. (2002). Involvement of continental crust in the formation of the Cretaceous Kerguelen Plateau: New perspectives from ODP Leg 120 sites. *Journal of Petrology*, *43*(7), 1207–1239. https://doi.org/10.1093/petrology/43.7.1207

Galer, S., & O'nions, R. (1985). Residence time of thorium, uranium and lead in the mantle with implications for mantle convection. *Nature*, *316*(6031), 778–782. https://doi.org/10.1038/316778a0

Garapić, G., Jackson, M. G., Hauri, E. H., Hart, S. R., Farley, K. A., Blusztajn, J. S., & Woodhead, J. D. (2015). A radiogenic isotopic (He-Sr-Nd-Pb-Os) study of lavas from the Pitcairn hotspot: Implications for the origin of EM-1 (enriched mantle 1). *Lithos*, *228*, 1–11. https://doi.org/10.1016/j.lithos.2015.04.010

Geldmacher, J., Hoernle, K., Klügel, A., van den Bogaard, P., & Bindeman, I. (2008). Geochemistry of a new enriched mantle type locality in the northern hemisphere: Implications for the origin of the EM-I source. *Earth and Planetary Science Letters*, *265*(1–2), 167–182. https://doi.org/10.1016/j.epsl.2007.10.001

Gibson, S., Thompson, R., Day, J., Humphris, S., & Dickin, A. (2005). Melt-generation processes associated with the Tristan mantle plume: Constraints on the origin of EM-1. *Earth and Planetary Science Letters*, *237*(3–4), 744–767. https://doi.org/10.1016/j.epsl.2005.06.015

Hanan, B. B., Blichert-Toft, J., Pyle, D. G., & Christie, D. M. (2004). Contrasting origins of the upper mantle revealed by hafnium and lead isotopes from the Southeast Indian Ridge. *Nature*, *432*(7013), 91–94. https://doi.org/10.1038/nature03181

Hanski, E., Kamenetsky, V. S., Luo, Z. Y., Xu, Y. G., & Kuzmin, D. V. (2010). Primitive magmas in the Emeishan large igneous province, southwestern China and northern Vietnam. *Lithos*, *119*(1–2), 75–90. https://doi.org/10.1016/j.lithos.2010.04.008

Hanski, E., Walker, R. J., Huhma, H., Polyakov, G. V., Balykin, P. A., Hoa, T. T., & Phuong, N. T. (2004). Origin of the Permian-Triassic komatiites, northwestern Vietnam. *Contributions to Mineralogy and Petrology*, *147*(4), 453–469. https://doi.org/10.1007/s00410-004-0567-1

Hart, S. R., Blusztajn, J., Dick, H. J., Meyer, P. S., & Muehlenbachs, K. (1999). The fingerprint of seawater circulation in a 500-meter section of ocean crust gabbros. *Geochimica et Cosmochimica Acta*, *63*(23–24), 4059–4080. https://doi.org/10.1016/S0016-7037(99)00309-9

Hart, S. R., Hauri, E. H., Oschmann, L. A., & Whitehead, J. A. (1992). Mantle plumes and entrainment: Isotopic evidence. *Science*, *256*(5056), 517–520. https://doi.org/10.1126/science.256.5056.517

Hart, S. R., & Jackson, M. G. (2014). Ta'u and Ofu/Olosega volcanoes: The "Twin Sisters" of Samoa, their P, T, X melting regime, and global implications. *Geochemistry, Geophysics, Geosystems*, *15*, 2301–2318. https://doi.org/10.1002/2013GC005221

Hauri, E. H., Lassiter, J. C., & DePaolo, D. J. (1996). Osmium isotope systematics of drilled lavas from Mauna Loa, Hawaii. *Journal of Geophysical Research*, *101*(B5), 11793–11806. http://doi.org/10.1029/95JB03346

Hauri, E. H., Whitehead, J. A., & Hart, S. R. (1994). Fluid dynamic and geochemical aspects of entrainment in mantle plumes. *Journal of Geophysical Research*, *99*(B12), 24275–24300. https://doi.org/10.1029/94jb01257

He, B., Xu, Y. G., Chung, S. L., Xiao, L., & Wang, Y. (2003). Sedimentary evidence for a rapid, kilometer-scale crustal doming prior to the eruption of the Emeishan flood basalts. *Earth and Planetary Science Letters*, *213*(3–4), 391–405. https://doi.org/10.1016/s0012-821x(03)00323-6

He, Q., Xiao, L., Balta, B., Gao, R., & Chen, J. Y. (2010). Variety and complexity of the Late-Permian Emeishan basalts: Reappraisal of plume–lithosphere interaction processes. *Lithos*, *119*(1), 91–107. https://doi.org/10.1016/j.lithos.2010.07.020

Heinonen, J. S., Jennings, E. S., & Riley, T. R. (2015). Crystallisation temperatures of the most Mg-rich magmas of the Karoo LIP on the basis of Al-in-olivine thermometry. *Chemical Geology*, *411*, 26–35. https://doi.org/10.1016/j.chemgeo.2015.06.015

Hergt, J. M., Peate, D. W., & Hawkesworth, C. J. (1991). The petrogenesis of Mesozoic Gondwana low-Ti flood basalts. *Earth and Planetary Science Letters*, *105*(1–3), 134–148. https://doi.org/10.1016/0012-821X(91)90126-3

Herzberg, C., & Asimow, P. D. (2008). Petrology of some oceanic island basalts: PRIMELT2. XLS software for primary magma calculation. *Geochemistry, Geophysics, Geosystems*, *9*, Q090001. https://doi.org/10.1029/2008GC002057

Herzberg, C., & Asimow, P. D. (2015). PRIMELT3 MEGA. XLSM software for primary magma calculation: Peridotite primary magma MgO contents from the liquidus to the solidus. *Geochemistry, Geophysics, Geosystems*, *16*(2), 563–578. https://doi.org/10.1002/2014gc005631

Herzberg, C., & O'hara, M. J. (2002). Plume-associated ultramafic magmas of Phanerozoic age. *Journal of Petrology*, *43*(10), 1857–1883. https://doi.org/10.1093/petrology/43.10.1857

Hirose, K. (1997). Partial melt compositions of carbonated peridotite at 3 GPa and role of $CO_2$ in alkali–basalt magma generation. *Geophysical Research Letters*, *24*(22), 2837–2840. https://doi.org/10.1029/97GL02956

Hofmann, A. W. (1988). Chemical differentiation of the Earth: The relationship between mantle, continental crust, and oceanic crust. *Earth and Planetary Science Letters*, *90*(3), 297–314. https://doi.org/10.1016/0012-821x(88)90132-x

Hofmann, A. W. (1997). Mantle geochemistry: The message from oceanic volcanism. *Nature*, *385*(6613), 219–229. https://doi.org/10.1038/385219a0

Hofmann, A. W. (2003). Sampling mantle heterogeneity through oceanic basalts: Isotopes and trace elements. In R. W. Carlson (Ed.), *The mantle and core: Treatise on geochemistry* (*2* (pp. 61–101). Amsterdam: Elsevier. https://doi.org/10.1016/B0-08-043751-6/02123-X

Hofmann, A. W., Jochum, K. P., Seufert, M., & White, W. M. (1986). Nb and Pb in oceanic basalts: New constraints on mantle evolution. *Earth and Planetary Science Letters*, *79*(1–2), 33–45. https://doi.org/10.1016/0012-821X(86)90038-5

Hofmann, A. W., & White, W. M. (1982). Mantle plumes from ancient oceanic crust. *Earth and Planetary Science Letters*, *57*(2), 421–436. https://doi.org/10.1016/B0-08-043751-6/02123-X

Hou, T., Zhang, Z. C., Encarnacion, J., Santosh, M., & Sun, Y. L. (2013). The role of recycled oceanic crust in magmatism and metallogeny: Os–Sr–Nd isotopes, U–Pb geochronology and geochemistry of picritic dykes in the Panzhihua giant Fe–Ti oxide deposit, central Emeishan large igneous province, SW China. *Contributions to Mineralogy and Petrology*, *165*(4), 805–822. https://doi.org/10.1007/s00410-012-0836-3

Hou, T., Zhang, Z. C., Kusky, T., Du, Y. S., Liu, J. L., & Zhao, Z. D. (2011). A reappraisal of the high-Ti and low-Ti classification of basalts and petrogenetic linkage between basalts and mafic–ultramafic intrusions in the Emeishan large igneous province, SW China. *Ore Geology Reviews*, *41*(1), 133–143. https://doi.org/10.1016/j.oregeorev.2011.07.005

Huang, H., Du, Y. S., Yang, J. H., Zhou, L., Hu, L. S., Huang, H. W., & Huang, Z. Q. (2014). Origin of Permian basalts and clastic rocks in Napo, Southwest China: Implications for the erosion and eruption of the Emeishan large igneous province. *Lithos*, *208*, 324–338. https://doi.org/10.1016/j.lithos.2014.09.022

Jackson, M. G., Hart, S. R., Koppers, A. A., Staudigel, H., Konter, J., Blusztajn, J., et al. (2007). The return of subducted continental crust in Samoan lavas. *Nature*, *448*(7154), 684–687. https://doi.org/10.1038/nature06048

Jennings, E. S., Gibson, S. A., & Maclennan, J. (2019). Hot primary melts and mantle source for the Paraná-Etendeka flood basalt province: New constraints from Al-in-olivine thermometry. *Chemical Geology*, *529*, 119287. https://doi.org/10.1016/j.chemgeo.2019.119287

Jochum, K. P., Weis, U., Schwager, B., Stoll, B., Wilson, S. A., & Haug, G. H. (2011). GSD-1G and MPI-DING reference glasses for in situ and bulk isotopic determination. *Geostandards and Geoanalytical Research*, *35*(2), 193–226. http://doi.org/10.1111/j.1751-908X.2010.00114.x

Johnson, M. C., & Plank, T. (1999). Dehydration and melting experiments constrain the fate of subducted sediments. *Geochemistry, Geophysics, Geosystems*, *1*(12), 1007. https://doi.org/10.1029/1999GC000014

Jourdan, F., Bertrand, H., Schärer, U., Blichert-Toft, J., Féraud, G., & Kampunzu, A. (2007). Major and trace element and Sr, Nd, Hf, and Pb isotope compositions of the Karoo large igneous province, Botswana–Zimbabwe: Lithosphere vs mantle plume contribution. *Journal of Petrology*, *48*(6), 1043–1077. https://doi.org/10.1093/petrology/egm010

Kamenetsky, V. S., Chung, S. L., Kamenetsky, M. B., & Kuzmin, D. V. (2012). Picrites from the Emeishan large igneous province, SW China: A compositional continuum in primitive magmas and their respective mantle sources. *Journal of Petrology*, *53*(10), 2095–2113. https://doi.org/10.1093/petrology/egs045

Kamenetsky, V. S., Maas, R., Kamenetsky, M. B., Yaxley, G. M., Ehrig, K., Zellmer, G. F., et al. (2017). Multiple mantle sources of continental magmatism: Insights from "high-Ti" picrites of Karoo and other large igneous provinces. *Chemical Geology*, *455*, 22–31. http://doi.org/10.1016/j.chemgeo.2016.08.034

Kent, A. J. R. (2008). Melt inclusions in basaltic and related volcanic rocks. *Reviews in Mineralogy and Geochemistry*, *69*(1), 273–331. https://doi.org/10.2138/rmg.2008.69.8

Kent, A. J. R., Baker, J. A., & Wiedenbeck, M. (2002). Contamination and melt aggregation processes in continental flood basalts: Constraints from melt inclusions in Oligocene basalts from Yemen. *Earth and Planetary Science Letters*, *202*(3–4), 577–594. https://doi.org/10.1016/S0012-821X(02)00823-3

Lai, S. C., Qin, J. F., Li, Y. F., Li, S. Z., & Santosh, M. (2012). Permian high Ti/Y basalts from the eastern part of the Emeishan large igneous province, southwestern China: Petrogenesis and tectonic implications. *Journal of Asian Earth Sciences*, *47*, 216–230. https://doi.org/10.1016/j.jseaes.2011.07.010

Lassiter, J. C., & Hauri, E. H. (1998). Osmium-isotope variations in Hawaiian lavas: Evidence for recycled oceanic lithosphere in the Hawaiian plume. *Earth and Planetary Science Letters*, *164*(3–4), 483–496. http://doi.org/10.1016/s0012-821x(98)00240-4

Le Bas, M. J., Le Maitre, R. W., Streckeisen, A., & Zanettin, B. (1986). A chemical classification of volcanic rocks based on the total alkali-silica diagram. *Journal of Petrology*, *27*(3), 745–750. https://doi.org/10.1093/petrology/27.3.745

Lee, C. T. A., Peter, L., Tobias, H. I., Jie, L., Rajdeep, D., & John, H. (2010). Upside-down differentiation and generation of a 'primordial' lower mantle. *Nature*, *463*(7283), 930–933. https://doi.org/10.1038/nature08824

Li, Y. J., He, H. Y., Ivanov, A. V., Demonterova, E. I., Pan, Y. X., Deng, C. L., et al. (2017). $^{40}Ar/^{39}Ar$ age of the onset of high-Ti phase of the Emeishan volcanism strengthens the link with the end-Guadalupian mass extinction. *International Geology Review*, *60*(15), 1906–1917. https://doi.org/10.1080/00206814.2017.1405748

Liu, J., Xia, Q. K., Kuritani, T., Hanski, E., & Yu, H. R. (2017). Mantle hydration and the role of water in the generation of large igneous provinces. *Nature Communications*, *8*(1), 1824. https://doi.org/10.1038/s41467-017-01940-3

Liu, X. J., Liang, Q. D., Li, L. Z., Castillo, P. R., Shi, Y., Xu, J. F., et al. (2016). Origin of permian extremely high Ti/Y mafic lavas and dykes from western Guangxi, SW China: Implications for the Emeishan mantle plume magmatism. *Journal of Asian Earth Sciences*, *141*, 97–111. http://doi.org/10.1016/j.jseaes.2016.09.005

Maclennan, J. (2008a). Lead isotope variability in olivine-hosted melt inclusions from Iceland. *Geochimica et Cosmochimica Acta*, *72*(16), 4159–4176. http://doi.org/10.1016/j.gca.2008.05.034

Maclennan, J. (2008b). Concurrent mixing and cooling of melts under Iceland. *Journal of Petrology*, *49*(11), 1931–1953. https://doi.org/10.1093/petrology/egn052

Matthews, S., Shorttle, O., & Maclennan, J. (2016). The temperature of the Icelandic mantle from olivine–spinel aluminum exchange thermometry. *Geochemistry, Geophysics, Geosystems*, *17*, 4725–4752. https://doi.org/10.1002/2016GC006497

McCulloch, M. T., & Wasserburg, G. J. (1978). Sm-Nd and Rb-Sr chronology of continental crust formation. *Science*, *200*(4345), 1003–1011. https://doi.org/10.1126/science.200.4345.1003

McDonough, W. F., & Sun, S. S. (1995). The composition of the Earth. *Chemical Geology*, *120*(3–4), 223–253. https://doi.org/10.1016/0009-2541(94)00140-4

Mckenzie, D., & O'Nions, R. K. (1983). Mantle reservoirs and ocean island basalts. *Nature*, *301*(5897), 229–231. https://doi.org/10.1038/301229a0

Millot, R., Allègre, C. J., Gaillardet, J., & Roy, S. (2004). Lead isotopic systematics of major river sediments: A new estimate of the Pb isotopic composition of the upper continental crust. *Chemical Geology*, *203*(1–2), 75–90. http://doi.org/10.1016/j.chemgeo.2003.09.002

Nielsen, R. L., Crum, J., Bourgeois, R., Hascall, K., Forsythe, L. M., Fisk, M. R., & Christie, D. M. (1995). Melt inclusions in high-An plagioclase from the Gorda Ridge: An example of the local diversity of MORB parent magmas. *Contributions to Mineralogy and Petrology*, *122*(1–2), 34–50. https://doi.org/10.1007/s004100050111

Nielsen, R. L., Michael, P. J., & Sours-Page, R. (1998). Chemical and physical indicators of compromised melt inclusions. *Geochimica et Cosmochimica Acta*, *62*(5), 831–839. https://doi.org/10.1016/s0016-7037(98)00024-6

Nisbet, E. G., Cheadle, M. J., Arndt, N. T., & Bickle, M. J. (1993). Constraining the potential temperature of the Archaean mantle: A review of the evidence from komatiites. *Lithos*, *30*(3–4), 291–307. https://doi.org/10.1016/0024-4937(93)90042-B

Norman, M. D., Garcia, M. O., Kamenetsky, V. S., & Nielsen, R. L. (2002). Olivine-hosted melt inclusions in Hawaiian picrites: Equilibration, melting, and plume source characteristics. *Chemical Geology*, *183*(1–4), 143–168. https://doi.org/10.1016/S0009-2541(01)00376-X

Othman, D. B., White, W. M., & Patchett, J. (1989). The geochemistry of marine sediments, island arc magma genesis, and crust-mantle recycling. *Earth and Planetary Science Letters*, *94*(1–2), 1–21. https://doi.org/10.1016/0012-821X(89)90079-4

Paul, B., Woodhead, J. D., Hergt, J., Danyushevsky, L., Kunihiro, T., & Nakamura, E. (2011). Melt inclusion Pb-isotope analysis by LA–MC-ICPMS: Assessment of analytical performance and application to OIB genesis. *Chemical Geology*, *289*(3–4), 210–223. https://doi.org/10.1016/j.chemgeo.2011.08.005

Peterson, M., Saal, A., Nakamura, E., Kitagawa, H., Kurz, M., & Koleszar, A. (2014). Origin of the 'Ghost Plagioclase'Signature in Galapagos Melt Inclusions: New Evidence from Pb Isotopes. *Journal of Petrology*, *55*(11), 2193–2216. https://doi.org/10.1093/petrology/egu054

Plank, T. (2005). Constraints from thorium/lanthanum on sediment recycling at subduction zones and the evolution of the continents. *Journal of Petrology*, *46*(5), 921–944. https://doi.org/10.1093/petrology/egi005

Plank, T. (2014). The chemical composition of subducting sediments. In H. D. Hol-land, & K. K. Turekian (Eds.), *Treatise on geochemistry* (second edition), *4* (pp. 607–629). Amsterdam. Elsevier. https://doi.org/10.1016/B978-0-08-095975-7.00319-3

Plank, T., & Langmuir, C. H. (1998). The chemical composition of subducting sediment and its consequences for the crust and mantle. *Chemical Geology*, *145*(3–4), 325–394. https://doi.org/10.1016/S0009-2541(97)00150-2

Putirka, K. (2016). Rates and styles of planetary cooling on Earth, Moon, Mars, and Vesta, using new models for oxygen fugacity, ferric-ferrous ratios, olivine-liquid Fe-Mg exchange, and mantle potential temperature. *American Mineralogist*, *101*(4), 819–840. http://doi.org/10.2138/am-2016-5402

Putirka, K., Tao, Y., Hari, K. R., Perfit, M. R., Jackson, M. G., & Arevalo, J. R. (2018). The mantle source of thermal plumes: Trace and minor elements in olivine and major oxides of primitive liquids (and why the olivine compositions don't matter). *American Mineralogist*, *103*(8), 1253–1270. http://doi.org/10.2138/am-2018-6192

Putirka, K. D., Perfit, M., Ryerson, F. J., & Jackson, M. G. (2007). Ambient and excess mantle temperatures, olivine thermometry, and active vs. passive upwelling. *Chemical Geology*, *241*(3–4), 177–206.http://doi.org/j.chemgeo.2007.01.014

Qi, L., & Zhou, M. F. (2008). Platinum-group elemental and Sr-Nd-Os isotopic geochemistry of Permian Emeishan flood basalts in Guizhou Province, SW China. *Chemical Geology*, *248*(1–2), 83–103. http://doi.org/10.1016/j.chemgeo.2007.11.004

Ren, Z. Y., Ingle, S., Takahashi, E., Hirano, N., & Hirata, T. (2005). The chemical structure of the Hawaiian mantle plume. *Nature*, *436*(7052), 837–840. https://doi.org/10.1038/nature03907

Ren, Z. Y., Wu, Y. D., Zhang, L., Nichols, A. R., Hong, L. B., Zhang, Y. H., et al. (2017). Primary magmas and mantle sources of Emeishan basalts constrained from major element, trace element and Pb isotope compositions of olivine-hosted melt inclusions. *Geochimica et Cosmochimica Acta*, *208*, 63–85. https://doi.org/10.1016/j.gca.2017.01.054

Rose-Koga, E. F., Koga, K. T., Moreira, M., Vlastélic, I., Jackson, M. G., Whitehouse, M. J., et al. (2017). Geochemical systematics of Pb isotopes, fluorine, and sulfur in melt inclusions from São Miguel, Azores. *Chemical Geology*, *458*, 22–37. https://doi.org/10.1016/j.chemgeo.2017.03.024

Rose-Koga, E. F., Koga, K. T., Schiano, P., Le Voyer, M., Shimizu, N., Whitehouse, M. J., & Clocchiatti, R. (2012). Mantle source heterogeneity for South Tyrrhenian magmas revealed by Pb isotopes and halogen contents of olivine-hosted melt inclusions. *Chemical Geology*, *334*, 266–279. https://doi.org/10.1016/j.chemgeo.2012.10.033

Rudnick, R. L., & Fountain, D. M. (1995). Nature and composition of the continental crust: A lower crustal perspective. *Reviews of Geophysics*, *33*(3), 267–309. http://doi.org/10.1029/95rg01302

Rudnick, R. L., & Gao, S. (2003). Composition of the continental crust. In H. D. Hol-land, & K. K. Turekian (Eds.), *Treatise on geochemistry*, (*3*, (p. 659). Amsterdam. Elsevier. https://doi.org/10.1016/B0-08-043751-6/03016-4

Saal, A. E., Hart, S. R., Shimizu, N., Hauri, E. H., Layne, G. D., & Eiler, J. M. (2005). Pb isotopic variability in melt inclusions from the EMI–EMII–HIMU mantle end-members and the role of the oceanic lithosphere. *Earth and Planetary Science Letters*, *240*(3–4), 605–620. https://doi.org/10.1016/j.epsl.2005.10.002

Sakyi, P. A., Tanaka, R., Kobayashi, K., & Nakamura, E. (2012). Inherited Pb isotopic records in olivine antecryst-hosted melt inclusions from Hawaiian lavas. *Geochimica et Cosmochimica Acta*, *95*, 169–195. https://doi.org/10.1016/j.gca.2012.07.025

Schiavi, F., Kobayashi, K., Nakamura, E., Tiepolo, M., & Vannucci, R. (2012). Trace element and Pb–B–Li isotope systematics of olivine-hosted melt inclusions: Insights into source metasomatism beneath Stromboli (southern Italy). *Contributions to Mineralogy and Petrology*, *163*(6), 1011–1031. https://doi.org/10.1007/s00410-011-0713-5

Schmidt, M. W., & Weidendorfer, D. (2018). Carbonatites in oceanic hotspots. *Geology*, *46*(5), 435–438. https://doi.org/10.1130/G39621.1

Shellnutt, J. G. (2014). The Emeishan large igneous province: A synthesis. *Geoscience Frontiers*, *5*(3), 369–394. https://doi.org/10.1016/j.gsf.2013.07.003

Shellnutt, J. G., & Jahn, B. M. (2010). Formation of the Late Permian Panzhihua plutonic-hypabyssal-volcanic igneous complex: Implications for the genesis of Fe–Ti oxide deposits and A-type granites of SW China. *Earth and Planetary Science Letters*, *289*(3–4), 509–519. https://doi.org/10.1016/j.epsl.2009.11.044

Shellnutt, J. G., & Jahn, B. M. (2011). Origin of Late Permian Emeishan basaltic rocks from the Panxi region (SW China): Implications for the Ti-classification and spatial–compositional distribution of the Emeishan flood basalts. *Journal of Volcanology and Geothermal Research*, *199*(1–2), 85–95. https://doi.org/10.1016/j.jvolgeores.2010.10.009

Shellnutt, J. G., Pham, T. T., Denyszyn, S. W., Yeh, M. W., & Tran, T. A. (2020). Magmatic duration of the Emeishan large igneous province: Insight from northern Vietnam. *Geology*, *48*(5), 457–461. https://doi.org/10.1130/G47076.1

Shellnutt, J. G., Zhou, M. F., & Zellmer, G. F. (2009). The role of Fe–Ti oxide crystallization in the formation of A-type granitoids with implications for the Daly gap: An example from the Permian Baima igneous complex, SW China. *Chemical Geology*, *259*(3–4), 204–217. https://doi.org/10.1016/j.chemgeo.2008.10.044

Shorttle, O., Maclennan, J., & Lambart, S. (2014). Quantifying lithological variability in the mantle. *Earth and Planetary Science Letters*, *395*, 24–40. http://doi.org/10.1016/j.epsl.2014.03.040

Sobolev, A. V. (1996). Melt inclusions in minerals as a source of principle petrological information. *Petrology*, *4*(3), 209–220. https://doi.org/10.1144/petgeo.2.2.185

Sobolev, A. V., Hofmann, A. W., Jochum, K. P., Kuzmin, D. V., & Stoll, B. (2011). A young source for the Hawaiian plume. *Nature*, *476*(7361), 434–437. https://doi.org/10.1038/nature10321

Sobolev, A. V., Hofmann, A. W., Kuzmin, D. V., Yaxley, G. M., Arndt, N. T., Chung, S. L., et al. (2007). The amount of recycled crust in sources of mantle-derived melts. *Science*, *316*(5823), 412–417. https://doi.org/10.1126/science.1138113

Sobolev, A. V., Hofmann, A. W., & Nikogosian, I. K. (2000). Recycled oceanic crust observed in 'ghost plagioclase'within the source of Mauna Loa lavas. *Nature*, *404*(6781), 986–990. https://doi.org/10.1038/35010098

Sobolev, A. V., & Shimizu, N. (1993). Ultra-depleted primary melt included in an olivine from the Mid-Atlantic Ridge. *Nature*, *363*(6425), 151–154. http://doi.org/10.1038/363151a0

Song, X. Y., Qi, H. W., Hu, R. Z., Chen, L. M., Yu, S. Y., & Zhang, J. F. (2013). Formation of thick stratiform Fe-Ti oxide layers in layered intrusion and frequent replenishment of fractionated mafic magma: Evidence from the Panzhihua intrusion, SW China. *Geochemistry, Geophysics, Geosystems*, *14*, 712–732. https://doi.org/10.1002/ggge.20068

Song, X. Y., Qi, H. W., Robinson, P. T., Zhou, M. F., Cao, Z. M., & Chen, L. M. (2008). Melting of the subcontinental lithospheric mantle by the Emeishan mantle plume; evidence from the basal alkaline basalts in Dongchuan, Yunnan, Southwestern China. *Lithos*, *100*(1–4), 93–111. https://doi.org/10.1016/j.lithos.2007.06.023

Song, X. Y., Zhou, M. F., Hou, Z. Q., Cao, Z. M., Wang, Y. L., & Li, Y. (2001). Geochemical constraints on the mantle source of the upper Permian Emeishan continental flood basalts, southwestern China. *International Geology Review*, *43*(3), 213–225. http://doi.org/10.1080/00206810109465009

Sours-Page, R., Johnson, K. T., Nielsen, R. L., & Karsten, J. L. (1999). Local and regional variation of MORB parent magmas: Evidence from melt inclusions from the Endeavour Segment of the Juan de Fuca Ridge. *Contributions to Mineralogy and Petrology*, *134*(4), 342–363. https://doi.org/10.1007/s004100050489

Sours-Page, R., Nielsen, R. L., & Batiza, R. (2002). Melt inclusions as indicators of parental magma diversity on the northern East Pacific Rise. *Chemical Geology*, *183*(1–4), 237–261. https://doi.org/10.1016/S0009-2541(01)00384-9

Staudigel, H., Plank, T., White, B., & Schmincke, H. U. (1996). Geochemical fluxes during seafloor alteration of the basaltic upper crust: DSDP sites 417 and 418. In G. E. Bebout, D. W. Scholl, S. H. Kirby, & J. P. Platt (Eds.), *Subduction: Top to bottom*, *96* (pp. 19–38). Washington, DC. American Geophysical Union. https://doi.org/10.1029/GM096p0019

Stracke, A. (2012). Earth's heterogeneous mantle: A product of convection-driven interaction between crust and mantle. *Chemical Geology*, *330*, 274–299. https://doi.org/10.1016/j.chemgeo.2012.08.007

Stracke, A., Bizimis, M., & Salters, V. J. (2003). Recycling oceanic crust: Quantitative constraints. *Geochemistry, Geophysics, Geosystems*, *4*(3), 8003. https://doi.org/10.1029/2001GC000223

Stracke, A., Hofmann, A. W., & Hart, S. R. (2005). FOZO, HIMU, and the rest of the mantle zoo. *Geochemistry, Geophysics, Geosystems*, *6*, Q05007. https://doi.org/10.1029/2004GC000824

Sun, S. S., & McDonough, & W. F. (1989). Chemical and isotopic systematics of oceanic basalts: Implications for mantle composition and processes. *Geological Society, London, Special Publications*, *42*(1), 313–345. https://doi.org/10.1144/GSL.SP.1989.042.01.19

Tanaka, T., Togashi, S., Kamioka, H., Amakawa, H., Kagami, H., Hamamoto, T., et al. (2000). JNdi-1: A neodymium isotopic reference in consistency with LaJolla neodymium. *Chemical Geology*, *168*(3–4), 279–281. https://doi.org/10.1016/S0009-2541(00)00198-4

Tao, Y., Putirka, K., Hu, R. Z., & Li, C. S. (2015). The magma plumbing system of the Emeishan large igneous province and its role in basaltic magma differentiation in a continental setting. *American Mineralogist*, *100*(11–12), 2509–2517. https://doi.org/10.2138/am-2015-4907

Teng, F. Z., Li, W. Y., Ke, S., Marty, B., Dauphas, N., Huang, S. C., et al. (2010). Magnesium isotopic composition of the earth and chondrites. *Geochimica et Cosmochimica Acta*, *74*(14), 4150–4166. https://doi.org/10.1016/j.gca.2010.04.019

Tian, H. C., Yang, W., Li, S. G., & Ke, S. (2017). Could sedimentary carbonates be recycled into the lower mantle? Constraints from Mg isotopic composition of Emeishan basalts. *Lithos*, *292*, 250–261. https://doi.org/10.1016/j.lithos.2017.09.007

Todt, W., Cliff, R. A., Hanser, A., & Hofmann, A. (1996). Evaluation of a $^{202}$Pb-$^{205}$Pb double spike for high-precision lead isotope analysis. In A. Basu, & S. R. Hart (Eds.), *Earth processes: Reading the isotopic code* (*95* (pp. 429–437). Washington, DC. American Geophysical Union. https://doi.org/10.1029/GM095p0429

Turner, S. J., Langmuir, C. H., Dungan, M. A., & Escrig, S. (2017). The importance of mantle wedge heterogeneity to subduction zone magmatism and the origin of EM1. *Earth and Planetary Science Letters*, *472*, 216–228. https://doi.org/10.1016/j.epsl.2017.04.051

Valer, M., Schiano, P., & Bachèlery, P. (2017). Geochemical characteristics of the La Réunion mantle plume source inferred from olivine-hosted melt inclusions from the adventive cones of Piton de la Fournaise volcano (La Réunion Island). *Contributions to Mineralogy and Petrology*, *172*(9), 74. https://doi.org/10.1007/s00410-017-1397-2

Vance, D., & Thirlwall, M. (2002). An assessment of mass discrimination in MC-ICPMS using Nd isotopes. *Chemical Geology*, *185*(3–4), 227–240. https://doi.org/10.1016/S0009-2541(01)00402-8

Vervoort, J. D., Plank, T., & Prytulak, J. (2011). The Hf–Nd isotopic composition of marine sediments. *Geochimica et Cosmochimica Acta*, *75*(20), 5903–5926. https://doi.org/10.1016/j.gca.2011.07.046

Wang, C. Y., Zhou, M. F., & Qi, L. (2007). Permian flood basalts and mafic intrusions in the Jinping (SW China)–Song Da (northern Vietnam) district: Mantle sources, crustal contamination and sulfide segregation. *Chemical Geology*, *243*(3–4), 317–343. https://doi.org/10.1016/j.chemgeo.2007.05.017

Wang, X. J., Chen, L. H., Hofmann, A. W., Hanyu, T., Kawabata, H., Zhong, Y., et al. (2018). Recycled ancient ghost carbonate in the Pitcairn mantle plume. *Proceedings of the National Academy of Sciences*, *115*(35), 8682–8687. https://doi.org/10.1073/pnas.1719570115

Weaver, B. L. (1991). The origin of ocean island basalt end-member compositions: Trace element and isotopic constraints. *Earth and Planetary Science Letters*, *104*(2–4), 381–397. https://doi.org/10.1016/0012-821x(91)90217-6

Weaver, B. L., Wood, D. A., Tarney, J., & Joron, J. L. (1986). Role of subducted sediment in the genesis of ocean-island basalts: Geochemical evidence from South Atlantic Ocean islands. *Geology*, *14*(4), 275–278. https://doi.org/10.1130/0091-7613(1986)142.0.CO;2

Weis, D., Kieffer, B., Maerschalk, C., Pretorius, W., & Barling, J. (2005). High-precision Pb-Sr-Nd-Hf isotopic characterization of USGS BHVO-1 and BHVO-2 reference materials. *Geochemistry, Geophysics, Geosystems*, *6*, Q02002. https://doi.org/10.1029/2004GC000852

White, W. M. (2010). Oceanic island basalts and mantle plumes: The Geochemical perspective. *Annual Review of Earth and Planetary Sciences*, *38*, 133–160. https://doi.org/10.1146/annurev-earth-040809-152450

White, W. M., & Hofmann, A. W. (1982). Sr and Nd isotope geochemistry of oceanic basalts and mantle evolution. *Nature*, *296*(5860), 821–825. https://doi.org/10.1038/296821a0

Wignall, P. B., Sun, Y. D., Bond, D. P. G., Izon, G., Newton, R. J., Védrine, S., et al. (2009). Volcanism, mass extinction, and carbon isotope fluctuations in the Middle Permian of China. *Science*, *324*(5931), 1179–1182. https://doi.org/10.1126/science.1171956

Willbold, M., & Stracke, A. (2006). Trace element composition of mantle end-members: Implications for recycling of oceanic and upper and lower continental crust. *Geochemistry, Geophysics, Geosystems*, 7, Q04004. https://doi.org/10.1029/2005GC001005

Willbold, M., & Stracke, A. (2010). Formation of enriched mantle components by recycling of upper and lower continental crust. *Chemical Geology*, *276*(3–4), 188–197. http://doi.org/10.1016/j.chemgeo.2010.06.005

Woodhead, J. D., Greenwood, P., Harmon, R. S., & Stoffers, P. (1993). Oxygen isotope evidence for recycled crust in the source of EM-type ocean island basalts. *Nature*, *362*(6423), 809–813. http://doi.org/10.1016/10.1038/362809a0

Workman, R. K., Hart, S. R., Jackson, M., Regelous, M., Farley, K., Blusztajn, J., et al. (2004). Recycled metasomatized lithosphere as the origin of the Enriched Mantle II (EM2) end-member: Evidence from the Samoan Volcanic Chain. *Geochemistry, Geophysics, Geosystems*, *5*(4), Q04008. https://doi.org/10.1029/2003GC000623

Wu, F. Y., Yang, Y. H., Xie, L. W., Yang, J. H., & Xu, P. (2006). Hf isotopic compositions of the standard zircons and baddeleyites used in U-Pb geochronology. *Chemical Geology*, *234*(1–2), 105–126. https://doi.org/10.1016/j.chemgeo.2006.05.003

Wu, Y. D., Ren, Z. Y., Handler, M. R., Zhang, L., Qian, S. P., Xu, Y. G., et al. (2018). Melt diversity and magmatic evolution in the Dali Picrites, Emeishan large igneous province. *Journal of Geophysical Research: Solid Earth*, *123*, 9635–9657. https://doi.org/10.1029/2018JB015495

Xiao, L., Xu, Y. G., Mei, H. J., Zheng, Y. F., He, B., & Pirajno, F. (2004). Distinct mantle sources of low-Ti and high-Ti basalts from the western Emeishan large igneous province, SW China: Implications for plume–lithosphere interaction. *Earth and Planetary Science Letters*, *228*(3), 525–546. http://doi.org/10.1016/j.epsl.2004.10.002

Xie, X. J., Yan, M. C., Wang, C. S., Li, L. Z., & S, H. J. (1989). Geochemical standard reference samples GSD 9-12, GSS 1-8 and GSR 1-6. *Geostandards Newsletter*, *13*(1), 83–179. http://doi.org/10.1111/j.1751-908X.1989.tb00469.x

Xu, J. F., Suzuki, K., Xu, Y. G., Mei, H. J., & Li, J. (2007). Os, Pb, and Nd isotope geochemistry of the Permian Emeishan continental flood basalts: Insights into the source of a large igneous province. *Geochimica et Cosmochimica Acta*, *71*(8), 2104–2119. http://doi.org/10.1016/j.gca.2007.01.027

Xu, R., & Liu, Y. S. (2016). Al-in-olivine thermometry evidence for the mantle plume origin of the Emeishan large igneous province. *Lithos*, *266*, 362–366. https://doi.org/10.1016/j.lithos.2016.10.016

Xu, R., Liu, Y. S., & Lambart, S. (2020). Melting of a hydrous peridotite mantle source under the Emeishan large igneous province. *Earth-Science Reviews*, *207*, 103253. http://doi.org/10.1016/j.earscirev.2020.103253

Xu, Y. C., Yang, Z. Y., Tong, Y. B., & Jing, X. Q. (2018). Paleomagnetic secular variation constraints on the rapid eruption of the Emeishan continental flood basalts in southwestern China and northern Vietnam. *Journal of Geophysical Research: Solid Earth*, *123*, 2597–2617. https://doi.org/10.1002/2017JB014757

Xu, Y. G., Chung, S. L., Jahn, B. M., & Wu, G. (2001). Petrologic and geochemical constraints on the petrogenesis of Permian–Triassic Emeishan flood basalts in southwestern China. *Lithos*, *58*(3–4), 145–168. https://doi.org/10.1016/S0024-4937(01)00055-X

Xu, Y. G., Chung, S. L., Shao, H., & He, B. (2010). Silicic magmas from the Emeishan large igneous province, Southwest China: Petrogenesis and their link with the end-Guadalupian biological crisis. *Lithos*, *119*(1–2), 47–60. https://doi.org/10.1016/j.lithos.2010.04.013

Xu, Y. G., He, B., Chung, S. L., Menzies, M. A., & Frey, F. A. (2004). Geologic, geochemical, and geophysical consequences of plume involvement in the Emeishan flood-basalt province. *Geology*, *32*(10), 917–920. https://doi.org/10.1130/G20602.1

Xu, Y. G., Mei, H. J., Xu, J., Huang, X. L., Wang, Y. J., & Chung, S. L. (2003). Origins of two different trends in the Emeishan flood basalts. *Chinese Science Bulletin*, *48*(4), 390–394. https://doi.org/10.1360/03tb9082

Yang, C., & Liu, S. A. (2019). Zinc isotope constraints on recycled oceanic crust in the mantle sources of the Emeishan large igneous province. *Journal of Geophysical Research: Solid Earth*, *124*, 12537–12555. https://doi.org/10.1029/2019JB017405

Yang, J., Cawood, P. A., & Du, Y. S. (2015). Voluminous silicic eruptions during Late Permian Emeishan igneous province and link to climate cooling. *Earth and Planetary Science Letters*, *432*, 166–175. https://doi.org/10.1130/G20602.1

Yao, J. H., Zhu, W. G., Li, C., Zhong, H., Yu, S., Ripley, E. M., & Bai, Z. J. (2019). Olivine O isotope and trace element constraints on source variation of picrites in the Emeishan flood basalt province, SW China. *Lithos*, *338*, 87–98. https://doi.org/10.1016/j.lithos.2019.04.019

Yu, S. Y., Chen, L. M., Lan, J. B., He, Y. S., Chen, Q., & Song, X. Y. (2020). Controls of mantle source and condition of melt extraction on generation of the picritic lavas from the Emeishan large igneous province, SW China. *Journal of Asian Earth Sciences*, *203*, 104534. http://doi.org/10.1016/j.jseaes.2020.104534

Yu, S. Y., Shen, N. P., Song, X. Y., Ripley, E. M., Li, C., & Chen, L. M. (2017). An integrated chemical and oxygen isotopic study of primitive olivine grains in picrites from the Emeishan large igneous province, SW China: Evidence for oxygen isotope heterogeneity in mantle sources. *Geochimica et Cosmochimica Acta*, *215*, 263–276. https://doi.org/10.1016/j.gca.2017.08.007

Yu, S. Y., Song, X. Y., Chen, L. M., & Li, X. B. (2014). Postdated melting of subcontinental lithospheric mantle by the Emeishan mantle plume: Evidence from the Anyi intrusion, Yunnan, SW China. *Ore Geology Reviews*, *57*, 560–573. https://doi.org/10.1016/j.oregeorev.2013.08.006

Yurimoto, H., Kogiso, T., Abe, K., Barsczus, H. G., Utsunomiya, A., & Maruyama, S. (2004). Lead isotopic compositions in olivine-hosted melt inclusions from HIMU basalts and possible link to sulfide components. *Physics of the Earth and Planetary Interiors*, *146*(1–2), 231–242. https://doi.org/10.1016/j.pepi.2003.08.013

Zhang, L., Ren, Z. Y., Handler, M. R., Wu, Y. D., Zhang, L., Qian, S. P., et al. (2019). The origins of high-Ti and low-Ti magmas in large igneous provinces, insights from melt inclusion trace elements and Sr–Pb isotopes in the Emeishan large Igneous Province. *Lithos*, *344*, 122–133. https://doi.org/10.1016/j.lithos.2019.06.014

Zhang, L., Ren, Z. Y., Nichols, A. R. L., Zhang, Y. H., Zhang, Y., Qian, S. P., & Liu, J. Q. (2014). Lead isotope analysis of melt inclusions by LA-MC-ICP-MS. *Journal of Analytical Atomic Spectrometry*, *29*(8), 1939–1405. https://doi.org/10.1039/C4JA00088A

Zhang, Y., Ren, Z. Y., & Xu, Y. G. (2013). Sulfur in olivine-hosted melt inclusions from the Emeishan picrites: Implications for S degassing and its impact on environment. *Journal of Geophysical Research: Solid Earth*, *118*(18), 4063–4070. https://doi.org/10.1002/jgrb.50324

Zhang, Z. C., Mahoney, J. J., Mao, J. W., & Wang, F. S. (2006). Geochemistry of picritic and associated basalt flows of the western Emeishan flood basalt province, China. *Journal of Petrology*, *47*(10), 1997–2019. https://doi.org/10.1093/petrology/egl034

Zhang, Z. C., Zhi, X., Chen, L., Saunders, A. D., & Reichow, M. K. (2008). Re–Os isotopic compositions of picrites from the Emeishan flood basalt province, China. *Earth and Planetary Science Letters*, *276*(1–2), 30–39. https://doi.org/10.1016/j.epsl.2008.09.005

Zhao, L., Guo, F., Fan, W. M., & Huang, M. W. (2019). Roles of subducted pelagic and terrigenous sediments in Early Jurassic mafic magmatism in NE China: Constraints on the architecture of Paleo-Pacific subduction zone. *Journal of Geophysical Research: Solid Earth*, *124*, 2525–2550. https://doi.org/10.1029/2018JB016487

Zhong, H., Qi, L., Hu, R. Z., Zhou, M. F., Gou, T. Z., Zhu, W. G., et al. (2011). Rhenium–osmium isotope and platinum-group elements in the Xinjie layered intrusion, SW China: Implications for source mantle composition, mantle evolution, PGE fractionation and mineralization. *Geochimica et Cosmochimica Acta*, *75*(6), 1621–1641. https://doi.org/10.1016/j.gca.2011.01.009

Zhong, Y. T., He, B., Mundil, R., & Xu, Y. G. (2014). CA-TIMS zircon U–Pb dating of felsic ignimbrite from the Binchuan section: Implications for the termination age of Emeishan large igneous province. *Lithos*, *204*, 14–19. https://doi.org/10.1016/j.lithos.2014.03.005

Zhong, Y. T., Mundil, R., Chen, J., Yuan, D. X., Denyszyn, S. W., Jost, A. B., et al. (2020). Geochemical, biostratigraphic, and high-resolution geochronological constraints on the waning stage of Emeishan large igneous province. *Geological Society of America Bulletin*, *132*(9–10), 1969–1986. https://doi.org/10.1130/B35464.1

Zhou, M. F., Arndt, N. T., Malpas, J., Wang, C. Y., & Kennedy, A. K. (2008). Two magma series and associated ore deposit types in the Permian Emeishan large igneous province, SW China. *Lithos*, *103*(3–4), 352–368. https://doi.org/10.1016/j.lithos.2007.10.006

Zhou, M. F., Zhao, J. H., Qi, L., Su, W. C., & Hu, R. Z. (2006). Zircon U-Pb geochronology and elemental and Sr–Nd isotope geochemistry of Permian mafic rocks in the Funing area, SW China. *Contributions to Mineralogy and Petrology*, *151*(1), 1–19. https://doi.org/10.1007/s00410-005-0030-y

Zhu, J., Zhang, Z. C., Reichow, M. K., Li, H. B., Cai, W. C., & Pan, R. H. (2018). Weak vertical surface movement caused by the ascent of the Emeishan mantle anomaly. *Journal of Geophysical Research: Solid Earth*, *123*, 1018–1034. https://doi.org/10.1002/2017JB015058